

Two Extraordinary Substellar Binaries at the T/Y Transition and the Y -Band Fluxes of the Coolest Brown Dwarfs^{1,2}

Michael C. Liu,^{3,4} Trent J. Dupuy,^{5,6} Brendan P. Bowler,³ S. K. Leggett,⁷ William M. J. Best³

ABSTRACT

Using Keck laser guide star adaptive optics imaging, we have found that the T9 dwarf WISE J1217+1626 and T8 dwarf WISE J1711+3500 are exceptional binaries, with unusually wide separations ($\approx 0.8''$, 8–15 AU), large near-IR flux ratios (≈ 2 –3 mags), and small mass ratios (≈ 0.5). Keck/NIRSPEC H -band spectra give a spectral type of Y0 for WISE J1217+1626B, and photometric estimates suggest T9.5 for WISE J1711+3500B. The WISE J1217+1626AB system is very similar to the T9+Y0 binary CFBDSIR J1458+1013AB; these two systems are the coldest known substellar multiples, having secondary components of ≈ 400 K and being planetary-mass binaries if their ages are $\lesssim 1$ Gyr. Both WISE J1217+1626B and CFBDSIR J1458+1013B have strikingly blue $Y - J$ colors compared to previously known T dwarfs, including their T9 primaries. Combining all available data, we find that $Y - J$ color drops precipitously between the very latest T dwarfs and the Y dwarfs. The fact that this is seen in the (co-eval, mono-metallicity) binaries WISE J1217+1626AB and CFBDSIR J1458+1013AB

¹Most of the data presented herein were obtained at the W.M. Keck Observatory, which is operated as a scientific partnership among the California Institute of Technology, the University of California, and the National Aeronautics and Space Administration. The Observatory was made possible by the generous financial support of the W.M. Keck Foundation.

²Some of the observations were obtained at the Gemini Observatory, which is operated by the Association of Universities for Research in Astronomy, Inc., under a cooperative agreement with the NSF on behalf of the Gemini partnership: the National Science Foundation (United States), the Science and Technology Facilities Council (United Kingdom), the National Research Council (Canada), CONICYT (Chile), the Australian Research Council (Australia), Ministério da Ciência, Tecnologia e Inovação (Brazil) and Ministerio de Ciencia, Tecnología e Innovación Productiva (Argentina).

³Institute for Astronomy, University of Hawaii, 2680 Woodlawn Drive, Honolulu HI 96822

⁴Visiting Astronomer at the Infrared Telescope Facility, which is operated by the University of Hawaii under Cooperative Agreement no. NNX-08AE38A with the National Aeronautics and Space Administration, Science Mission Directorate, Planetary Astronomy Program.

⁵Harvard-Smithsonian Center for Astrophysics, 60 Garden Street, Cambridge, MA 02138

⁶Hubble Fellow

⁷Gemini Observatory, 670 North A'ohoku Place, Hilo, HI 96720

demonstrates that the color drop arises from a change in temperature, not surface gravity or metallicity variations among the field population. Thus, the T/Y transition established by near-IR spectra coincides with a significant change in the $\approx 1 \mu\text{m}$ fluxes of ultracool photospheres. One explanation is the depletion of potassium, whose broad absorption wings dominate the far-red optical spectra of T dwarfs. This large color change suggests that far-red data may be valuable for classifying objects of $\lesssim 500$ K.

Subject headings: binaries: general, close — stars: brown dwarfs — infrared: stars — techniques: high angular resolution

1. Introduction

Binaries have played a central role in the study of the coolest dwarfs over the last two decades. Each advance that has led to creation of a later spectral type has benefitted from discovery of companions to higher mass objects. The first L dwarf, GD 165B, was found as a companion to a white dwarf (Becklin & Zuckerman 1988). At the time, its unusual optical spectrum compared to late-M dwarfs was puzzling, but with the subsequent discovery of more L dwarfs, it became apparent that GD 165B was the prototype of a new spectral type (Kirkpatrick et al. 1999). The first T dwarf, Gl 229B, was found around an M dwarf (Nakajima et al. 1995), and its uniqueness was evident from the strong CH_4 and H_2O in its near-IR spectrum (Oppenheimer et al. 1995).

Just last year, two low-mass companions were found with temperatures of only $\approx 300\text{--}400$ K, one being a tight (3 AU) companion to the T9.5 dwarf CFBDSIR J1458+1013 (Liu et al. 2011) and the other being a very wide (2500 AU) companion to the white dwarf GJ 3483 (Luhman et al. 2011). Spectroscopy of these objects has not been possible yet, due to the small angular separation (0.11") of CFBDSIR J1458+1013AB and the lack of a near-IR detection for GJ 3483B (a.k.a. WD 0806–661B). However, their exceptionally faint absolute magnitudes clearly showed these two objects were novel compared to all previously known T dwarfs. Their temperatures, as inferred from their absolute magnitudes using evolutionary models, are far cooler than the previous record-holder, the ≈ 520 K T10 dwarf UGPS J0722–0540 (Lucas et al. 2010), and place the two companions in *terra incognita* where theoretical models predict the onset of new photospheric signatures including NH_3 absorption in the near-IR, the disappearance of neutral alkali lines, and the formation of water clouds (Burrows et al. 2003). More recently, Cushing et al. (2011) have identified five free-floating objects with sufficiently distinct near-IR spectra to propose classification as Y dwarfs, based on the likely presence of NH_3 absorption in the blue wing of their *H*-band continua. While reliable parallaxes are not yet available for these objects and thus their absolute magnitudes are uncertain, model atmosphere fits indicate temperatures of $\approx 300\text{--}500$ K. Their novel near-IR appearance may be a precursor to even more significant changes along the remaining temperature gap down to Jupiter (124 K; Guillot 2005).

As part of our ongoing effort to study low-temperature objects using substellar binaries, we

present here the discovery of two extraordinarily well-resolved binaries that shed light on the transition from the latest T dwarfs to the Y dwarfs. The primaries, WISEPC J121756.91+162640.2 and WISEPA J171104.60+350036.8 (hereinafter WISE J1217+1626 and WISE J1711+3500), were found from a mid-IR search of the solar neighborhood by Kirkpatrick et al. (2011), who assigned integrated-light near-IR spectral types of T9 and T8, respectively. We also present improved near-IR imaging of CFBDSIR J1458+1013AB. Our characterization of these three binaries includes resolved photometry in the Y band, which spans the $\approx 1.0 \mu\text{m}$ transmission window of the Earth’s atmosphere. A broadband filter in this window is a new capability for adaptive optics imaging at Keck, just installed in September 2011. One of the prime motivating factors for its procurement, as a collaboration between one of us (M. Liu) and Keck Observatory, is to explore the $\approx 1 \mu\text{m}$ fluxes of the coolest brown dwarfs, which can be diagnostic of surface gravity, metallicity, and photospheric chemistry (e.g. Leggett et al. 2012).

2. Observations

2.1. Keck-II/NIRC2 Adaptive Optics Imaging

We imaged WISE J1217+1626, WISE J1711+3500, and CFBDSIR J1458+1013 over 3 nights in January and April 2012 using the laser guide star adaptive optics (LGS AO) system of the 10-meter Keck II Telescope on Mauna Kea, Hawaii (Wizinowich et al. 2006; van Dam et al. 2006). For WISE J1217+1626, we used the facility IR camera NIRC2 with its wide field-of-view optics ($40.8'' \times 40.8''$), and for WISE J1711+3500 and CFBDSIR J1458+1013 we used the narrow field-of-view optics ($10.2'' \times 10.2''$). Conditions were photometric, with $0.8''$ seeing in January and $0.4\text{--}0.6''$ seeing in April. The LGS provided the wavefront reference source for AO correction, with the tip-tilt motion measured contemporaneously using $R = 15.5$, 14.4 , and 15.5 mag stars from the USNO-B1.0 catalog (Monet et al. 2003) located $38''$, $43''$, and $55''$ away from WISE J1217+1626, WISE J1711+3500, and CFBDSIR J1458+1013, respectively. The LGS brightness, as measured by the flux incident on the AO wavefront sensor, was equivalent to a $V \approx 9.5\text{--}10.0$ mag star. The LGS was pointed at the center of the NIRC2 field-of-view for all observations.

We obtained images with all or a subset of the broad-band Y ($1.02 \mu\text{m}$), J ($1.25 \mu\text{m}$), H ($1.64 \mu\text{m}$), and K ($2.20 \mu\text{m}$) filters of the Mauna Kea Observatories (MKO) photometric system (Simons & Tokunaga 2002; Tokunaga et al. 2002). We also obtained data with the medium-band $CH4s$ filter (central wavelength of $1.592 \mu\text{m}$, $0.126 \mu\text{m}$ wide), which is positioned around the H -band peak in the spectra of T dwarfs. Finally, for WISE J1217+1626, we obtained data with NIRC2’s custom “ z ” filter (central wavelength of $1.031 \mu\text{m}$, $0.048 \mu\text{m}$ wide), which covers the cleanest portion of the Y -band atmospheric window. To avoid confusion with optical filters using the same letter but spanning different wavelengths, we refer to this as the $z_{1.1}$ filter.

For each filter, we obtained a set of dithered images, offsetting the telescope by a few arcseconds between every pair of images. The images were analyzed in the same fashion as our previous work

(e.g. Liu et al. 2006, 2008). The raw images were reduced using standard methods for flat-fielding and sky-subtraction. The binary’s flux ratios and relative astrometry were derived by fitting an analytic model of the point spread function as the sum of three elliptical gaussians.

For the very well-resolved *WISE* binaries, we fitted all the individual images and adopted the averages of the results as the final measurements and the standard deviations as the errors. (The two *WISE* binaries are so wide that simple aperture photometry gave essentially the same results, as the contamination of the secondary by the primary is negligible.) For CFBDSIR J1458+1013AB, we fitted the stacked mosaic to maximize the S/N of the faint, close secondary and derived uncertainties from Monte Carlo simulations, as we did in Liu et al. (2011). For NIRC2’s wide camera, we adopted a pixel scale of 39.884 ± 0.039 mas/pixel and an orientation for the detector’s $+y$ axis of $0.16 \pm 0.09^\circ$ (Pravdo et al. 2006). For the narrow camera, we adopted a pixel scale of 9.963 ± 0.005 mas/pixel and an orientation for the detector’s $+y$ axis of $0.13 \pm 0.07^\circ$ (Ghez et al. 2008). The relative astrometry was corrected for (the very small) instrumental optical distortion based on a solution by B. Cameron (priv. comm.).

Table 1 presents our final measurements, and Figure 1 shows our reduced images. For all three binaries, the astrometry from the different filters shows excellent agreement. For *WISE* J1217+1626, our measurements have χ^2 values of 0.89 and 3.46 (5 degrees of freedom) for the separation and PA, respectively, when compared to the hypothesis of a constant value for each quantity. For *WISE* J1711+3500, the χ^2 values are 0.2 and 3.10 (4 degrees of freedom) for separation and PA, respectively, and for CFBDSIR J1458+1013AB they are 2.3 and 0.17 (2 degrees of freedom). Also, our CFBDSIR J1458+1013AB J and $CH4s$ flux ratios are consistent with those obtained in 2010 by Liu et al. (2011), with the new J -band data being a significant improvement. Given that the uncertainties in the resolved measurements are likely dominated by systematic errors in deblending the two components of this tight binary, we forgo averaging the 2010 and 2012 measurements and simply choose for each filter the measurement with the smaller error in our analysis (Section 3).

2.2. Gemini/NIRI Photometry of *WISE* J1217+1626

We obtained seeing-limited Y - and K -band integrated-light photometry of *WISE* J1217+1626AB using the facility near-IR camera NIRI (Hodapp et al. 2003) on the Gemini-North 8.1-m telescope on Mauna Kea, Hawaii. These observations complement the J - and H -band photometry published in Kirkpatrick et al. (2011). Our NIRI observations were obtained as queue observing program GN-2012A-DD-2 on 01 April 2012 UT. The seeing was $0.7''$ FWHM, and the binary was marginally resolved. We obtained five 60-s exposures at Y -band and eighteen 30-s exposures at K -band, taken using a dither pattern with $10''$ offsets. Data were reduced in a standard fashion and flatfielded with calibration lamps on the telescope. For photometric calibration, we observed the UKIRT faint standard FS 21, using K -band magnitudes from Leggett et al. (2006) and Y -band magnitudes from

the UKIRT online catalog.¹ We measured $Y_{NIRI} = 18.55 \pm 0.03$ mag and $K = 18.80 \pm 0.04$ mag for the integrated-light system. As discussed in the Appendix, we apply a small shift to transform the NIRI Y -band photometry to the MKO system, giving a final value of $Y_{MKO} = 18.38 \pm 0.04$ mag.

2.3. Keck-II/NIRSPEC Spectroscopy of WISE J1217+1626

We obtained resolved seeing-limited spectroscopy of WISE J1217+1626AB with the facility near-IR spectrograph NIRSPEC (McLean et al. 1998) on the Keck-II Telescope on 12 April 2012 UT. Seeing conditions were excellent, with 0.5–0.7'' FWHM in the optical as measured from the DIMM at the nearby Canada-France-Hawaii Telescope, suitable to resolve the two components of the binary. Very light cirrus was present in the sky. We used the low spectral resolution mode with the $0.38'' \times 42''$ slit and the NIRSPEC-5 blocking filter, which spans the H -band. The achieved spectral resolution ($\lambda/\delta\lambda$) was 2300 ± 200 based on measurements of bright isolated sky emission lines. The slit was oriented along the binary PA which did not match the parallactic angle. However, the binary was observed at airmass 1.0–1.1 so systematic errors due to differential chromatic refraction were negligible.

We obtained 12 exposures of WISE J1217+1626AB, each with a 300 s integration time, nodding the telescope in an ABBA fashion. Immediately afterwards, we observed the A0V star HD 109055 for telluric calibration and then obtained calibration observations of an internal flat-field source, argon arc lamps, and a dark frame. During the spectroscopic observations of both the science target and A0V calibrator, the NIRSPEC image quality was afflicted by an unusual guiding program, causing the formation of double-peaked PSFs in the spatial direction on the detector. The PSF's secondary peak was typically about 2/3 the flux of the main peak and in the direction opposite the binary's B component.

Basic image reduction was performed with the REDSPEC reduction package.² This included bad pixel removal, spatial rectification of the images, the creation of a wavelength solution, pairwise image subtraction, and flat fielding. Residual sky line emission in the pair-subtracted images was removed by subtracting a constant value at each wavelength as measured from a spatial region 10 pixels in width on either side of the target spectrum.

Because of the close separation of the binary pair and the unusual double-peaked PSF, we extracted 1-d spectra from the 2-d rectified images using custom IDL routines. We found that modeling the PSF as the sum of two gaussians provided an excellent match to the data. The 2-gaussian PSF of the two binary components differed only in total flux and position, as we fixed the FWHM and the relative amplitude of the 2 gaussians to be the same for each binary component. To determine the PSF characteristics of each image, we fit this 2-gaussian PSF model to the collapsed

¹http://www.jach.hawaii.edu/UKIRT/astrometry/calib/phot_cal/fs_ZY_MKO_wfcam.dat

²<http://www2.keck.hawaii.edu/inst/nirspec/redspec>

1.55–1.60 μm spatial profile of the individual reduced images using the nonlinear, least-squares curve fitting package MPFIT written in IDL (Markwardt 2009). The fitting results were used to fix all parameters of the PSF except the flux ratio of the binary. This model was then fit to the spatial profile as a function of wavelength, while median-averaging the spectrum in wavelength bins to boost the S/N. We found this model to be an excellent fit to the data, as the subtraction of a 2-d image based on the model fits from the original data produced essentially a pure noise image, without any coherent residuals.

The resulting individual spectra for WISE J1217+1626 A and B were computed at each wavelength bin by summing the flux of their respective 2-gaussian PSFs. To construct the final spectra, we combined the individual extracted spectra by first scaling each one to the median-averaged spectrum from 1.55–1.65 μm . Then at each wavelength we computed the weighted average, with the weights inversely proportional to the FWHM of the PSF model. The purpose of the weighting is to favor data obtained in better seeing conditions. We adopted the standard error of the individual spectra as the measurement uncertainties for the final spectrum.

The spectra of the A0V calibrator star were extracted by summing flux in a single fixed-sized aperture and then combined. This was used to correct the spectra of WISE J1217+1626A and B for telluric absorption using the `xtellcor_general` routine in the Spextool reduction package for IRTF (Cushing et al. 2004; Vacca et al. 2003). To test the sensitivity of the results to the fitting procedure, we experimented with wavelength bin sizes of 5, 10, 15, and 20 pixels (0.0014, 0.0028, 0.0042, 0.0055 μm). We also extracted the spectra by allowing the FWHM of each gaussian in the 2-gaussian PSF model vary. The results were all consistent within the spectral measurement uncertainties. We use the 10-pixel binned data for our final analysis, as the resulting sampling gives a resolution ($R \approx 200$) compared to other published near-IR spectra of late-T and Y dwarfs.

Figure 2 shows the reduced spectra of the two components. The peak S/N are about 60 and 15 for the primary and secondary, respectively. As a cross-check on our reduction, we also compare the sum of our spectra with the integrated-light spectrum from Kirkpatrick et al. (2011) and find excellent agreement, as shown in the inset of Figure 2. We also compute an H -band flux ratio from our NIRSPEC spectra of 2.25 ± 0.08 mag, in accord with our Keck LGS imaging (2.20 ± 0.04 mag).

2.4. IRTF/SpeX Photometry and Spectroscopy of WISE J1711+3500

To improve upon the modest S/N data for WISE J1711+3500 presented in Kirkpatrick et al. (2011), we obtained near-IR photometry and low-resolution ($R \approx 100$) spectroscopy of WISE J1711+3500. Such data are important for our analysis, since the Keck LGS imaging provides only flux ratios for the two components. Computing the resolved magnitudes requires multi-band integrated-light photometry, which can be synthesized from a near-IR spectrum and photometry in a single band.

We used the facility instrument SpeX (Rayner et al. 1998) at NASA’s Infrared Telescope Facility located on Mauna Kea, Hawaii on 2012 April 20 UT. For imaging, we obtained 9 dithered

exposures of WISE J1711+3500 and the UKIRT faint standard FS 27 using the MKO J -band filter. Conditions were photometric with good seeing, 0.6–0.7'' FWHM in J -band as measured from the reduced images. Data were reduced in a standard fashion, and we used aperture photometry to determine an apparent magnitude of $J_{MKO} = 17.59 \pm 0.03$ mag, with the uncertainty determined from the quadrature sum of the standard error of the fluxes from the individual images of the science target and photometric calibrator. Kirkpatrick et al. (2011) reported $J_{2MASS} = 17.89 \pm 0.13$ mag, which is consistent with our measurement given the ≈ 0.3 mag offset expected for late-T dwarfs between the MKO and 2MASS filter systems (Stephens & Leggett 2004). Our near-IR spectrum (described below) finds $J_{2MASS} - J_{MKO} = 0.26$ mag, consistent with the 0.30 ± 0.13 mag difference between our photometry and that of Kirkpatrick et al.

For spectroscopy, we used Spex in prism mode with the 0.8'' slit, obtaining 0.8–2.5 μm spectra in a single order. WISE J1711+3500 was nodded along the slit in an ABBA pattern with individual exposure times of 180 sec for a total exposure time of 48 min and observed over an airmass range of 1.04–1.06. We observed the A0V star GAT 7 (Gatewood & Eichhorn 1973) contemporaneously for telluric calibration. All spectra were reduced using version 3.4 of the SpeXtool software package (Vacca et al. 2003; Cushing et al. 2004). The S/N per pixel in the final reduced spectrum is about 35, 50, 25, and 8 in the $YJHK$ peaks, respectively. Figure 3 shows that our spectrum agrees well with that of Kirkpatrick et al. (2011). We use our spectrum and J -band photometry to synthesize the integrated-light magnitudes in the YHK bands on the MKO system (Table 3).

3. Results

3.1. Evidence for Companionship

With only one epoch of imaging, it is not possible to determine if the companions seen in the Keck LGS images are co-moving with the our two *WISE* targets. But the resolved photometry of the systems (and spectra in the case of WISE J1217+1626AB) provides overwhelming circumstantial evidence that the binaries are true physical associations. Specifically, the nearly identical flux ratios in the CH_4s and H -band images indicates that the secondary components also have strong methane absorption, with basically no flux redward of the 1.6 μm flux decrement seen in T dwarfs. The possibility of two unassociated T dwarfs having such a small angular separation is diminishingly small. Burningham et al. (2008, 2010) identified 54 T dwarfs in an area of 700 degs² to a depth of $J = 19.0$ mag. Nine of these objects are spectral type T7 or later, where the H -band methane absorption is saturated in medium-band filter photometry (Figure 4 of Liu et al. 2008). Assuming a uniform space density of late-T dwarfs, this means a surface density of 0.20 late-T dwarfs per degs⁻² to a depth of $J = 21.0$ mag. Within the field of view of the NIRC2 wide and narrow cameras, this corresponds to probabilities of 2.6×10^{-5} and 1.6×10^{-6} for an unassociated T dwarf to be next to WISE J1217+1626 and WISE J1711+3500, respectively. This is highly unlikely.

Note that this calculation is an *a posteriori* one based on a discovery of a companion to a

individual target. In fact, we need to consider the total number of objects that we have imaged with sensitivity to late-T dwarf companions. Our Keck LGS program to date (e.g. Liu et al. 2006, 2010, 2011) has targeted about 100 field T dwarfs using the NIRC2 narrow camera. Thus the probability of an unassociated late-T companion being contiguous to any single object in our survey is 1.6×10^{-4} , respectively. However, note that both these “single-object” and “total-survey” calculations overstate the odds of a chance association, since they do not consider that the photometric distance of a background late-T dwarf would not be compatible with those of the science targets. We conclude that both *WISE* systems are physical binaries.

We searched for common proper motion companions within $10'$ of WISE J1217+1626, using the proper motion reported in Kirkpatrick et al. (2011). We found no comoving objects in the Hipparcos, Tycho, LSPM-N, or NLTT catalogs. The reported proper motion of WISE J1711+3500 is consistent with zero, obviating a search for comoving companions.

3.2. Photometric Distances

We can estimate photometric distances to our two binaries using the late-T primary components, and then as a result we also know the distances to the T/Y secondary components. To compute a photometric distance for WISE J1217+1626AB, we compare the apparent magnitudes of component A to the six T8.5 and T9 dwarfs with parallaxes summarized in Dupuy & Liu (2012) and using the Cushing et al. (2011) spectral types for the latest T dwarfs. We include the T8.5 dwarfs (1) to compensate for the small sample of only two T9 dwarfs with parallaxes and MKO near-IR photometry (UGPS J0722–0540 and CFBDSIR J1458+1013A, which differ from each other by ≈ 0.9 mag in absolute magnitudes) and (2) to encompass the current uncertainties in the spectral typing of the very coolest brown dwarfs. A weighted average of the absolute magnitudes gives $M(Y, J, H, K) = 18.74 \pm 0.38, 17.88 \pm 0.35, 18.21 \pm 0.34, 18.42 \pm 0.39$ mag, where the uncertainty here is the RMS scatter of the six objects. We use the *J*- and *H*-band data for the photometric distance, as the *Y* and *K* bands are more influenced by variations in metallicity and surface gravity (e.g. Leggett et al. 2007; Liu et al. 2007). Both bands give an identical distance modulus of $(m - M) = 0.10 \pm 0.35$ mag (10.5 ± 1.7 pc) for WISE J1217+1626A.

In a similar fashion, for WISE J1711+3500AB we use the Dupuy & Liu (2012) weighted average of *J*- and *H*-band absolute magnitudes for T8 dwarfs, choosing the three objects that are “normal” (not young or low metallicity). These give distance moduli of 1.35 ± 0.35 and 1.41 ± 0.32 mag, respectively. We take the average and adopt the slightly larger RMS for a final distance modulus of 1.38 ± 0.35 mag (19 ± 3 pc) for WISE J1711+3500A.

As expected, our photometric distances are larger than the 6.7 pc and 17.0 pc estimates for WISE J1217+1626 and WISE J1711+3500, respectively, given by Kirkpatrick et al. (2011) which were based on integrated-light *W*2-band photometry assuming a single object. Note that if the large flux ratios we observe in the near-IR (≈ 2 – 3 mag) were also representative of the mid-IR flux

ratios, we would expect better agreement between our distances and those of Kirkpatrick et al. In other words, the secondary components in these systems must be relatively brighter in the mid-IR and thus contribute a larger portion of the $W2$ -band flux, as expected based on the very red mid-IR colors of the coolest brown dwarfs (e.g. Leggett et al. 2010b).

3.3. Spectral Types

3.3.1. *WISE J1217+1626AB*

Our NIRSPEC spectra of both components of WISE J1217+1626AB exhibit the deep H_2O and CH_4 absorption in the H -band that is characteristic of the coolest brown dwarfs. Figure 4 compares our H -band spectra with the T9 and Y0 spectroscopic standards proposed by Cushing et al. (2011). Component A shows excellent agreement with their T9 standard UGPS J0722–0540. The spectral type for this component is identical to the integrated-light type, as expected given the large near-IR flux ratios.

Component B shows good match with the Y0 standard WISE J1738+2732. In particular, the hallmark of the Y spectral type proposed by Cushing et al. (2011) is the enhanced absorption at 1.53–1.58 μm seen in the low-resolution spectra of the coolest *WISE* discoveries that is distinct from the latest T dwarfs. They attribute this feature to NH_3 , though a definitive identification is still pending. As seen in Figure 4, WISE J1217+1626B shows the same enhanced absorption on the blue side as the Y0 standard, and thus we classify it as Y0.

The red side of the H -band continuum for WISE J1217+1626B does not appear to be as sharply truncated as for the Y0 standard. However, the other Y0 dwarf from the Cushing et al. (2011) with reasonable S/N, WISE J1405+5534, also has a similar redward extent, which motivated a classification of “Y0 (pec?)” in their discovery paper. Given the modest S/N of our spectrum, we defer a decision on whether WISE J1217+1626B is spectroscopically peculiar. Followup resolved spectroscopy with broader wavelength coverage will help refine the spectral typing, especially as the width of the J -band continuum appears to decrease with later-type objects.

3.3.2. *WISE J1711+3500AB*

In the absence of resolved spectroscopy for WISE J1711+3500AB, we consider the flux ratios and estimated absolute magnitudes of the components to estimate their spectral types. The large near-IR flux ratios (≈ 2.8 mag) suggests strongly that the T8 integrated-light spectrum is dominated by the primary. This is corroborated with simple numerical experiments combining spectra of late-T and Y0 dwarfs using the observed H -band flux ratio as a constraint. The $>10\times$ fainter secondary has negligible impact on the near-IR spectrum. Thus we safely classify WISE J1711+3500A as T8.

For the secondary, we use its near-IR absolute magnitude as estimated from the photometric distance to the primary. This is obviously an uncertain process, though preliminary parallaxes from Kirkpatrick et al. (2012) suggest that the near-IR absolute magnitudes drop off quickly at the T/Y transition, which lessens the impact of uncertainties in the photometric distance. WISE J1711+3500B has $M(H) = 19.58 \pm 0.36$ mag, which is intermediate between the two T9 and two Y0 dwarfs with parallaxes in Figure 12 of Kirkpatrick et al. (2012). (Their figure has CFBDSIR J1458+1013B plotted as the sole T9.5, but as discussed in the next subsection this object is more likely to be typed as Y0.) In terms of its $Y - J$ color and estimated color-magnitude diagram position, WISE J1711+3500B also appears to be intermediate between the T9 and Y0 dwarfs (Section 3.4). Thus we estimate a spectral type of T9.5.

3.3.3. CFBDSIR J1458+1013AB

At the time CFBDSIR J1458+1013AB was discovered to be a binary, the near-IR absolute magnitudes of its secondary component were fainter than the coolest known dwarf, UGPS J0722–0540 which was classified as T10 at the time (Lucas et al. 2010). This motivated an initial spectral type estimate of $>T10$ for the secondary, with the primary type assumed to be identical to the integrated-light type of T9.5. While the secondary type was unknown given the absence of resolved spectroscopy, the monotonic behavior of near-IR absolute magnitudes among the T dwarfs demonstrated the object was exceptionally low temperature. Since then, there have been several late-T and Y dwarfs identified from the *WISE* dataset, which has warranted a reclassification of the integrated-light spectrum to T9 by Cushing et al. (2011). Given this new state of knowledge, we reexamine here the resolved spectral types.

Based on the latest H -band absolute magnitudes from Dupuy & Liu (2012), Kirkpatrick et al. (2011) estimated types of T8.5 and T9.5 for the two components of CFBDSIR J1458+1013AB. However, closer examination of the data indicates these types are too early. As is the case with WISE J1711+3500A, the large near-IR flux ratios (≈ 2 mag) of CFBDSIR J1458+1013AB indicate the T9 integrated-light spectrum is dominated by the primary. This is corroborated by the aforementioned experiments of summing spectra and by the model atmosphere fitting in Liu et al. (2011), which found a blended-light spectrum had negligible impact on the derived physical parameters. As for the secondary, its $M(H) = 19.99 \pm 0.23$ is in very good agreement with the two Y0 dwarfs in Kirkpatrick et al. (2012) with parallaxes. This absolute magnitude also agrees well with that estimated for the Y0 dwarf WISE J1217+1626B (based on a photometric distance for WISE J1217+1626A). Thus we conclude the most accurate spectral type estimates for the components of CFBDSIR J1458+1013AB are T9 and Y0.

3.4. Resolved Photometry

Tables 2, 3, and 4 summarize the resolved photometry for our binaries, derived from the Keck LGS imaging and the available $YJHK$ integrated-light photometry. Figure 5 shows the YJH color-color plot comparing our binary sample to the known field T dwarfs. For the field sample, we use the data for 80 T dwarfs compiled by Leggett et al. (2010b), one late-T dwarf (WISE J1617+1807) from Kirkpatrick et al. (2011),³ three recent late-T discoveries from the UKIDSS survey (Burningham et al. 2009; Lucas et al. 2010; Burningham et al. 2011), and one Y0 dwarf (WISE J1405+5534) from Morley et al. (2012).⁴ For the objects originally classified as T8.5–T10 in the Leggett et al. compilation, we use the slightly earlier spectral types of T8–T9 proposed by Cushing et al. (2011). We also queried the UKIDSS⁵ Large Area Survey Data Release 9 (DR9, Table 5) in order to add photometry for five late-T dwarfs from Kirkpatrick et al. and for the T8 dwarf PSO J043.5+02 (a.k.a. WISE J0254+0223, found independently by Scholz et al. 2011 and Liu et al. 2011). Finally, we computed YJH synthetic photometry for the six T9–T9.5 and two Y0 dwarfs (WISE J0410+1502 [Y0] and WISE J1541–2250 [Y0.5]) in Kirkpatrick et al. (2011) and Cushing et al. (2011) with sufficiently blue coverage in their spectra to include the Y -band.

While WISE J1217+1626A, WISE J1711+3500A, and WISE J1711+3500B reside in the loci of the coolest known objects, the unusual nature of WISE J1217+1626B is apparent in the YJH color-color diagram, being distinguished by its very blue $Y - J$ color compared to all previously known T dwarfs. Only the three field Y dwarfs in our sample are comparable. This blueness is also emphasized in the near-IR color-magnitude diagram (Figure 6), where component B is fainter and significantly bluer in $Y - J$ than any T dwarf, based on the photometric distance for the binary. The resolved $Y - J$ colors for CFBDISIR J1458+1013AB show a similarly pronounced blue difference between the primary and secondary component. This is seen most clearly in the relative flux ratios, $\Delta(Y - J) = 0.43 \pm 0.02$ mag for WISE J1217+1626AB and 0.47 ± 0.15 mag for CFBDISIR J1458+1013AB. (The integrated-light Y -band photometry for CFBDISIR J1458+1013AB is only $S/N = 5$ so comparing the resolved colors of the two components is more noisy than comparing their flux ratios, which depend only on the Keck LGS data.)

To further highlight this phenomenon, Figure 7 shows the $Y - J$ colors of the coolest brown

³The T9 dwarf WISE J1614+1739 in Kirkpatrick et al. also has YJH photometry but the resulting colors are unusual, with $Y - J = 0.35 \pm 0.12$ and $J - H = 0.61 \pm 0.22$ mag, which place it far from the color locus of all other T dwarfs. (The object would lie off the boundaries of Figure 5 to the upper left.). However, the near-IR spectrum appears similar to other late-T dwarfs, and synthetic photometry of the spectrum gives $Y - J = 0.77$ mag and $J - H = -0.26$ mag. Thus the photometry seems erroneous, so we exclude it.

⁴The Morley et al. Y -band photometry was obtained with Gemini/NIRI, so we apply the shift computed in the Appendix to transform it to the MKO system.

⁵UKIDSS (UKIRT Infrared Deep Sky Survey) is described in Lawrence et al. (2007). UKIDSS uses the UKIRT Wide Field Camera (WFCAM; Casali et al. 2007), and a photometric system described in Hewett et al. (2006). The pipeline processing and science archive are described in Dye et al. (2006) and Hambly et al. (2008).

dwarfs as a function of spectral type, based on published photometry and our synthesized photometry (regardless of whether the objects have parallaxes or not). Leggett et al. (2010b) and Burningham et al. (2010) have noted that the $Y - J$ colors of the latest T dwarfs (T8–T9) are bluer than the earlier-type objects, and Cushing et al. (2011) found that the Y -band peak of two Y0 dwarfs are relatively brighter compared to the T9 standard UGPS J0722–0540. Figure 7 shows that in fact the blueward trend in $Y - J$ crosses a precipice at the T/Y transition, declining dramatically (≈ 0.5 mag) over only half a spectral subclass, from T9.5 to Y0. This is discussed further in Section 4.

3.5. Physical Properties from Evolutionary Models

We use evolutionary models from Burrows et al. (2003) and Baraffe et al. (2003) to derive physical properties for the two binaries, assuming ages of 1 and 5 Gyr. As inputs, we use both the J -band absolute magnitude and the estimated L_{bol} . The uncertainties in these quantities are propagated into the calculations in a Monte Carlo fashion. We use J -band as it represents the peak flux of the near-IR spectral energy distribution. When using the J -band absolute magnitudes for our calculations, we are implicitly using the bolometric corrections from the underlying model atmospheres.

To compute L_{bol} , we adopt a J -band bolometric correction of 1.75 ± 0.27 mag for WISE J1217+1626A (T9), WISE J1217+1626B (Y0), and WISE J1711+3500B (\approx T9.5), based on the coolest T dwarfs as described in Liu et al. (2011). This is expected to somewhat underestimate the L_{bol} , given the increasingly large fraction of the luminosity emitted in the mid-IR at colder temperatures (e.g. Leggett et al. 2010b). However, given the lack of actual bolometric measurements for objects as cool as WISE J1217+1626B, adopting a fixed value is also conservative.

For the hotter WISE J1711+3500A (T8), we adopt J -band bolometric corrections from the four T7.5–T8.5 dwarfs with parallaxes: Gl 570D (T7.5; $BC_J = 2.60 \pm 0.13$ mag), 2MASS J1217–0311 (T7.5, 2.64 ± 0.13 mag), and 2MASS J0415–0935 (T8; 2.54 ± 0.13 mag) from Golimowski et al. (2004) and Wolf 940B (T8.5, 2.09 ± 0.12 mag) from Leggett et al. (2010a). The unweighted average and RMS are 2.47 ± 0.26 mag.

Tables 2 and 3 present the results derived from the evolutionary models. Altogether, the components of WISE J1217+1626AB are remarkably similar to those of CFBDSIR J1458+1013AB, with near-IR absolute magnitudes that differ by only ≈ 0.2 mag; thus, the inferred physical properties of these two systems are very similar. Note that the results from the Burrows et al. (2003) models should be somewhat preferred over the Lyon/COND models of Baraffe et al. (2003). The predicted near-IR locus of Burrows et al. is a better match to the location of CFBDSIR J1458+1013AB (Figure 7 of Liu et al. 2011), though the two sets of models basically give consistent results for the physical properties. Overall, the inferred temperature of WISE J1217+1626B is exceptionally low, 350–470 K depending on the choice of theoretical model and system age. Its inferred mass is 5–

20 M_{Jup} , overlapping the old gas-giant planets found by radial velocity and transit surveys and the young ones found by direct imaging (Chauvin et al. 2005; Lafrenière et al. 2008; Marois et al. 2008; Lagrange et al. 2010). As expected based on its brighter estimated absolute magnitudes, we find WISE J1711+3500B is somewhat hotter (420–540 K) and more massive (9–26 M_{Jup}) than WISE J1217+1626A.

Both components of WISE J1217+1626AB would reside in the planetary-mass regime and have retained their initial deuterium abundance for ages of $\lesssim 1$ Gyr. In fact, the two components of WISE J1217+1626AB may possess different deuterium abundances, as their estimated masses could straddle the deuterium-burning limit (11–14 M_{Jup} ; Spiegel et al. 2010). For WISE J1711+3500AB, the primary likely lies above the D-burning limit, and the secondary would lie below it for ages of $\lesssim 1$ Gyr. Measuring the differential deuterium abundance in these binaries would help constrain their ages, analogous to the binary lithium test proposed by Liu & Leggett (2005) — see Liu et al. (2011) for a discussion of the very similar case of CFBDSIR J1458+1013AB.

3.6. Orbital Period

To estimate the orbital period of the two new *WISE* binaries, we adopt the statistical conversion factor between projected separation and true semi-major axis from Dupuy & Liu (2011). They offer several choices, based on the underlying eccentricity distribution and degree of completeness to finding binaries by imaging (“discovery bias”). We adopt the eccentricity distribution from their compilation of ultracool visual binaries with high quality orbits and assume no discovery bias, appropriate for such well-resolved systems. This gives a multiplicative correction factor of $1.15^{+0.81}_{-0.31}$ (68.3% confidence limits) for converting the projected separation into semi-major axis (compared to $1.10^{+0.92}_{-0.35}$ for a uniform eccentricity distribution with no discovery bias). For ages of 1–5 Gyr, the resulting orbital period estimates range from 120–210 yr and 260–430 yr for the two binaries, albeit with significant uncertainties (Tables 2 and 3). Dynamical masses can be realized from orbit monitoring covering $\gtrsim 30\%$ of the period (e.g. Bouy et al. 2004; Liu et al. 2008; Dupuy et al. 2009). Thus, several decades of monitoring will be needed to determine the visual orbits.

Orbital motion of CFBDSIR J1458+1013AB is clearly detected in our new data, taken two years after the discovery epoch in Liu et al. (2011). Comparing the data from the filters with the best astrometry in the two epochs, we measure a change in separation of 16 ± 3 mas and in position angle of $8.5 \pm 1.6^\circ$. Such motion is not surprising, given the ≈ 30 yr orbital period estimated at the time of discovery.

4. Discussion

Theoretical models predict the near-IR spectra of ≈ 300 –500 K objects to be sensitive to new physical processes (e.g. Burrows et al. 2003; Leggett et al. 2007). Cushing et al. (2011) have identi-

fied changes in near-IR low-resolution spectra of Y dwarfs that they ascribe to NH_3 . This molecule may also be present in high-resolution near-IR spectra of UGPS J0722–0540 (Saumon et al. 2012a; Bochanski et al. 2011). Another anticipated signature is the removal of the very broad wings of the K I $0.77\ \mu\text{m}$ doublet that dominate the far-red optical continuum (e.g. Burrows et al. 2000; Marley et al. 2002). Down to $\approx 500\ \text{K}$, Leggett et al. (2012) find that the far-red colors, as tracked by the $izYJ$ filters, continue to be very red with only a hint of saturation.

At somewhat cooler temperatures, below $400\ \text{K}$ the Cs, K, Li and Rb neutral alkalis are expected to be depleted as they turn into chloride gases and solids, or other halide or hydroxide gases, and Na condenses as Na_2S (Lodders 1999; Leggett et al. 2012). Given the strength of the K I absorption wings, depletion of this element should be manifested by a change in the broad-band colors. Figures 5, 6, and 7 show that the $Y - J$ colors of WISE J1217+1626B and the other two Y dwarfs are significantly bluer than all known T dwarfs, consistent with the signature of such depletion. Indeed, the sharp change in $Y - J$ is reminiscent of similar behavior seen in near-IR JHK colors at the L/T transition due the onset of photospheric methane absorption (e.g. Knapp et al. 2004), though the change in $Y - J$ occurs over a small range of spectral subclasses.

Based on the photometric distance to its primary, the location of WISE J1217+1626B on the color-magnitude diagram also suggests a temperature low enough for potassium depletion. Figure 6 compares the available photometry with updated version of the Saumon & Marley (2008) models from D. Saumon (priv. comm.). These updated models include the latest H_2 collision-induced absorption and NH_3 opacities (Saumon et al. 2012b). However, the models are calculated in chemical equilibrium, which overestimates the strengths of the NH_3 absorption in the near-IR (which is significant) and the mid-IR assuming non-equilibrium conditions are prevalent, as expected. The cloud-free model sequences show $(Y - J)$ decreasing with decreasing temperature through the T dwarf sequence. The J -band absolute magnitudes of the Y0 dwarfs are comparable to the $\approx 400\ \text{K}$ models, though the observed $Y - J$ colors are somewhat bluer than the models. The predictions from Burrows et al. (2003) have much redder $Y - J$ colors than the color-magnitude data.

Note that the Saumon & Marley models include the formation of iron, silicate and corundum clouds (which are important for L dwarfs and the L/T transition) as well as the depletion of the neutral alkalis. However, they do not include any opacity due to sulphide or chloride condensates, such as Na_2S and KCl which are formed as Na and K are depleted. While such condensates have been historically ignored in ultracool atmosphere modeling, Morley et al. (2012) have found the resulting clouds, especially those of Na_2S , significantly affect the near-IR spectra of mid/late-T dwarfs and provide a better match to the JHK data. As shown in Figure 6, current cloud-free models agree reasonably well in $\{Y - J, M(J)\}$. But the mismatch for the latest-type objects may indicate that other factors in addition to $\text{K} \rightarrow \text{KCl}$ depletion play a role in the $\approx 1\ \mu\text{m}$ fluxes, including non-equilibrium NH_3 abundances and the opacity of sulfate condensates.

5. Conclusions

WISE J1217+1626AB and WISE J1711+3500AB are remarkably well-resolved binaries compared to previously known T dwarf binaries (Figure 8), with only the T1+T6 binary ϵ Ind Bab being comparably wide in angular separation ($0.73''$ at discovery; McCaughrean et al. 2004). The projected physical separations of 8 and 15 AU for the *WISE* binaries are also remarkable, with only the T2.5+T4.0 binary SIMP J1619275+031350AB being comparable (15 AU separation; Artigau et al. 2011) among T dwarfs. Finally, their mass ratios of ≈ 0.5 make them very rare among field ultracool binaries, where nearly equal-mass systems are most prevalent (e.g., see compilation in Liu et al. 2010). The fact that these two systems are so unusual in their separation and mass ratios compared to nearly all previously known substellar binaries opens the question of whether these initial discoveries among the late-T dwarfs is a harbinger of a change in binary properties at such cool temperatures. An answer awaits a larger survey of such targets at comparable sensitivity.

Overall, WISE J1217+1626AB appears to be essentially a clone of the coolest known binary to date, CFBDSIR J1458+1013AB, except for the difference in the projected separation. The blue $Y - J$ color of its secondary component is unmatched by any previously known T dwarf, including the primary component. Synthetic photometry of field Y0 dwarfs also gives very blue colors, and CFBDSIR J1458+1013B also shows a much bluer $Y - J$ color than its primary. Examining the complete ensemble of available $Y - J$ color data, we find a sharp drop to the blue between the T9.5 and Y0 dwarfs. We suggest this may be the signature of potassium depletion, which removes a significant opacity source at far-red optical wavelengths and is expected for objects of $\lesssim 400$ K. It is a fortuitous coincidence that the change in near-IR spectra that demarcates the T/Y transition (currently suspected to be due to NH_3) also coincides with this change in photospheric chemistry. However, in contrast to the relatively subtle changes in the near-IR spectra between T9 and Y0, the $Y - J$ color drops by ≈ 0.5 mag. This suggests that far-red spectra might be more discerning than near-IR spectra for classification in this temperature regime, as discussed by Leggett et al. (2007) and Liu et al. (2011).

Future followup will be essential for reaping the full scientific value of these new binaries. Near-IR low resolution spectra will readily improve the spectral types. Water clouds are also expected to condense below ≈ 400 K, further motivating detailed spectroscopic characterization to search for their signature. The wide separation of these two binaries means that resolved near-IR and optical spectra can be obtained in good seeing conditions, without the need for AO.

The binary nature of these systems also provides a unique avenue for analysis. Among the Y dwarfs, model atmosphere fitting (Cushing et al. 2011) indicates a significant range in temperatures (350–500 K), surface gravities (>1 dex range), and masses ($3\text{--}30 M_{\text{Jup}}$) that is in contrast to the modest differences in their near-IR spectra. It is unclear whether such dispersion represents intrinsic variations in the physical properties of Y dwarfs, failings in the model atmospheres, or both. For binaries, the two components have a common (albeit unknown) metallicity and very similar surface gravity (Tables 2 and 3). Thus resolved spectra will cleanly probe the effect of decreasing

temperature, without the uncertainties arising from second parameter variations (age/gravity or metallicity) present in the free-floating population. In a similar vein, spectrophotometric monitoring of the two components may shed light on the nature of the clouds at the T/Y transition.

Finally, the photometric distances of 10–20 pc place WISE J1217+1626AB and WISE J1711+3500AB easily within reach of near-IR parallax measurements, and we have begun such monitoring using the Canada-France-Hawaii Telescope (Dupuy & Liu 2012). A direct distance will place the four components in context with other late-T and Y dwarfs, through both the absolute magnitude-spectral type relation and color-magnitude diagrams. Given the unusually small mass ratios of ≈ 0.5 for these systems, placing the components on the H-R diagram will also uniquely test the joint accuracy of current evolutionary and atmospheric models, using the constraint that models must indicate the two components of each binary are coeval (Liu et al. 2010).

We thank Scott Dahm, Terry Stickel, Jim Lyke, and the Keck Observatory staff for assistance with LGS AO observing; the Gemini Observatory staff for obtaining the NIRI photometry through queue observing; and Kimberly Aller for assistance with the IRTF/SpeX observing. We thank Andrew Stephens for providing the Gemini/NIRI cold filter profile; James R. A. Davenport for distributing his IDL implementation of the Green (2011) “cubehelix” color scheme; Caroline Morley, Jonathan Fortney and collaborators for sharing results in advance of publication; and Didier Saumon and Isabelle Baraffe for providing expanded sets of evolutionary models. This publication makes use of data products from the Wide-Field Infrared Survey Explorer, which is a joint project of the University of California, Los Angeles, and the Jet Propulsion Laboratory/California Institute of Technology, funded by the National Aeronautics and Space Administration. Our research has employed the 2MASS data products; NASA’s Astrophysical Data System; the SIMBAD database operated at CDS, Strasbourg, France; and the SpeX Prism Spectral Libraries maintained by Adam Burgasser at <http://pono.ucsd.edu/~adam/browndwarfs/spexprism>. This research was supported by NSF grant AST09-09222 awarded to MCL. Finally, the authors wish to recognize and acknowledge the very significant cultural role and reverence that the summit of Mauna Kea has always had within the indigenous Hawaiian community. We are most fortunate to have the opportunity to conduct observations from this mountain.

Facilities: Keck-2 (LGS/NIRC2), Gemini-North (NIRI), IRTF (SpeX)

A. Y-Band Filter Offsets

The near-IR spectra of T dwarfs are highly structured and include strong absorption bands due to H_2O . These bands are proximate to the strong telluric absorption features in the Earth’s atmosphere. The telluric features have served to define the commonly used near-IR photometric bandpasses, though the exact wavelength ranges of the filters vary. Stephens & Leggett (2004) have computed photometric shifts between different near-IR filter systems in the ubiquitous *JHK* bands.

The shifts can be quite large (≈ 0.4 mag) depending on the particular filters being considered. The Y -band in the $\approx 1 \mu\text{m}$ atmospheric window is also subject to such effects.

The measurements in this paper involve Y -band photometry from three instruments: Keck/NIRC2 (resolved photometry of three binaries), Gemini/NIRI (integrated-light photometry of WISE J1217+1626AB), and UKIRT/WFCAM (integrated-light photometry of late-T dwarfs from the literature). The three filters are very similar, but they are distinct (Figure 9). The differences are especially significant for the late-T and Y dwarfs as the peak of their continuum in this bandpass falls near the red edge of the filter, so for a given object the Y -band magnitudes will be brightest for the UKIRT/WFCAM filter and faintest for the Keck/NIRC2 filter. To assess the offsets between filters, we synthesize colors in the various Y -band filters using spectra of T8– $Y0$ dwarfs with sufficient blue wavelength coverage, primarily from Kirkpatrick et al. (2011) and Cushing et al. (2011).

We compute a Gemini-UKIRT shift of $Y_{\text{NIRI}} - Y_{\text{WFCAM}} = 0.17 \pm 0.03$ mag, where the uncertainty is the RMS of the synthesized colors. We apply this small offset to our Gemini/NIRI photometry for a final value of $Y_{\text{MKO}} = 18.38 \pm 0.04$ mag for WISE J1217+1626AB (Table 2). We assume here that UKIRT/WFCAM serves as the de facto definition for the Y band of the MKO photometric system, given that the UKIDSS project carried out with this instrument has produced the largest set of Y -band photometry by far. Note that applying this shift does not affect one of our main results, namely the very blue ($Y - J$) color of WISE J1217+1626B compared to previously known objects, since the secondary is unusually blue relative to both the field objects and its T9 primary even if we apply no shift at all.

We also compute a Keck-UKIRT shift of $Y_{\text{NIRC2}} - Y_{\text{WFCAM}} = 0.27 \pm 0.03$ mag. Figure 9 indicates that for $Y0$ dwarfs, the WFCAM flux should be systematically different than for the Keck or Gemini fluxes given the stronger water absorption cutoff in the red edge of the bandpass for later-type objects, but no convincing offset was detected between the two Y dwarfs (WISE J0410+1502 and WISE J1541–2250) and the T8–T9.5 dwarfs in our compilation, especially given the low S/N spectra of the latest-type objects. Therefore, we assume the color offset has no spectral type dependence, and hence the flux ratios between the binary components in the Y_{NIRC2} and Y_{WFCAM} filters are assumed to be the same. If there is such a dependence, Figure 9 indicates that shifting from Keck/NIRC2 to UKIRT/WFCAM would make WISE J1217+1626B and CFBDSIR J1458+1013B even bluer relative to their primaries.

Finally, we synthesize the offsets between these Y -band filters over the entire T spectral class by adding the low-resolution spectra from the SpeX Prism Library. Figure 10 shows the results. Robust linear fitting to the synthetic photometry gives the following relations:

$$Y_{\text{NIRI}} - Y_{\text{WFCAM}} = 0.090 + 0.010 \times (T_{\text{subclass}}) \quad \sigma = 0.015 \text{ mag}$$

$$Y_{\text{NIRC2}} - Y_{\text{WFCAM}} = 0.133 + 0.017 \times (T_{\text{subclass}}) \quad \sigma = 0.019 \text{ mag}$$

$$Y_{\text{NIRC2}} - Y_{\text{NIRI}} = 0.042 + 0.007 \times (T_{\text{subclass}}) \quad \sigma = 0.006 \text{ mag}$$

where T_{subclass} is 0 for T0, 1 for T1, 10 for $Y0$, etc. and σ gives the RMS about the fitted relation.

REFERENCES

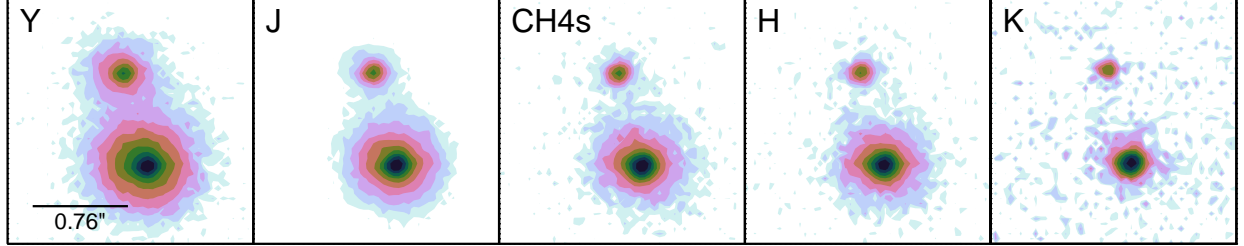
- Artigau, É., et al. 2011, *ApJ*, 739, 48
- Baraffe, I., Chabrier, G., Barman, T. S., Allard, F., & Hauschildt, P. H. 2003, *A&A*, 402, 701
- Becklin, E. E., & Zuckerman, B. 1988, *Nature*, 336, 656
- Bochanski, J. J., Burgasser, A. J., Simcoe, R. A., & West, A. A. 2011, *AJ*, 142, 169
- Bouy, H., et al. 2004, *A&A*, 423, 341
- Burningham, B., et al. 2008, *MNRAS*, 391, 320
- . 2009, *MNRAS*, 395, 1237
- . 2010, *MNRAS*, 406, 1885
- . 2011, *MNRAS*, 414, 3590
- Burrows, A., Marley, M. S., & Sharp, C. M. 2000, *ApJ*, 531, 438
- Burrows, A., Sudarsky, D., & Lunine, J. I. 2003, *ApJ*, 596, 587
- Casali, M., et al. 2007, *A&A*, 467, 777
- Chauvin, G., Lagrange, A.-M., Dumas, C., Zuckerman, B., Mouillet, D., Song, I., Beuzit, J.-L., & Lowrance, P. 2005, *A&A*, 438, L25
- Cushing, M. C., Vacca, W. D., & Rayner, J. T. 2004, *PASP*, 116, 362
- Cushing, M. C., et al. 2011, *ApJ*, 743, 50
- Delorme, P., et al. 2010, *A&A*, 518, A39
- Dupuy, T. J., & Liu, M. C. 2011, *ApJ*, 733, 122
- . 2012, *ArXiv e-prints*
- Dupuy, T. J., Liu, M. C., & Bowler, B. P. 2009, *ApJ*, 706, 328
- Gatewood, G., & Eichhorn, H. 1973, *AJ*, 78, 769
- Gelino, C. R., et al. 2011, *AJ*, in press (arXiv.org:1106.3142)
- Ghez, A. M., et al. 2008, *ApJ*, 689, 1044
- Golimowski, D. A., et al. 2004, *AJ*, 127, 3516
- Green, D. A. 2011, *Bulletin of the Astronomical Society of India*, 39, 289

- Guillot, T. 2005, *Annual Review of Earth and Planetary Sciences*, 33, 493
- Hambly, N. C., et al. 2008, *MNRAS*, 384, 637
- Hewett, P. C., Warren, S. J., Leggett, S. K., & Hodgkin, S. T. 2006, *MNRAS*, 367, 454
- Hodapp, K. W., et al. 2003, *PASP*, 115, 1388
- Kirkpatrick, J. D., Allard, F., Bida, T., Zuckerman, B., Becklin, E. E., Chabrier, G., & Baraffe, I. 1999, *ApJ*, 519, 834
- Kirkpatrick, J. D., et al. 2011, *ArXiv e-prints*
- Kirkpatrick, J. D., et al. 2012, *ArXiv e-prints*
- Knapp, G. R., et al. 2004, *AJ*, 127, 3553
- Lafrenière, D., Jayawardhana, R., & van Kerkwijk, M. H. 2008, *ApJ*, 689, L153
- Lagrange, A., et al. 2010, *Science*, 329, 57
- Lawrence, A., et al. 2007, *MNRAS*, 379, 1599
- Leggett, S. K., Saumon, D., Burningham, B., Cushing, M. C., Marley, M. S., & Pinfield, D. J. 2010a, *ApJ*, 720, 252
- Leggett, S. K., et al. 2006, *MNRAS*, 373, 781
- Leggett, S. K., et al. 2007, *ApJ*, 667, 537
- Leggett, S. K., et al. 2010b, *ApJ*, 710, 1627
- . 2012, *ApJ*, 748, 74
- Liu, M. C., et al. 2011, *ApJ*, 740, 108
- Liu, M. C., Dupuy, T. J., & Ireland, M. J. 2008, *ApJ*, 689, 436
- Liu, M. C., Dupuy, T. J., & Leggett, S. K. 2010, *ApJ*, 722, 311
- Liu, M. C., & Leggett, S. K. 2005, *ApJ*, 634, 616
- Liu, M. C., Leggett, S. K., & Chiu, K. 2007, *ApJ*, 660, 1507
- Liu, M. C., Leggett, S. K., Golimowski, D. A., Chiu, K., Fan, X., Geballe, T. R., Schneider, D. P., & Brinkmann, J. 2006, *ApJ*, 647, 1393
- Liu, M. C., et al. 2011, *ApJ*, 740, L32
- Lodders, K. 1999, *ApJ*, 519, 793

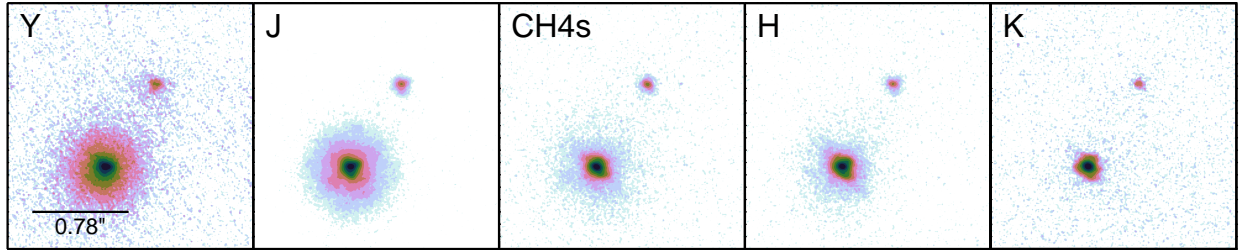
- Lucas, P. W., et al. 2010, *MNRAS*, 408, L56
- Luhman, K. L., Burgasser, A. J., & Bochanski, J. J. 2011, *ApJ*, 730, L9
- Markwardt, C. B. 2009, in *Astronomical Society of the Pacific Conference Series*, Vol. 411, *Astronomical Data Analysis Software and Systems XVIII*, ed. D. A. Bohlender, D. Durand, & P. Dowler, 251
- Marley, M. S., Seager, S., Saumon, D., Lodders, K., Ackerman, A. S., Freedman, R. S., & Fan, X. 2002, *ApJ*, 568, 335
- Marois, C., Macintosh, B., Barman, T., Zuckerman, B., Song, I., Patience, J., Lafrenière, D., & Doyon, R. 2008, *Science*, 322, 1348
- McCaughrean, M. J., Close, L. M., Scholz, R.-D., Lenzen, R., Biller, B., Brandner, W., Hartung, M., & Lodieu, N. 2004, *A&A*, 413, 1029
- McLean, I. S., et al. 1998, in *Proc. SPIE: Infrared Astronomical Instrumentation*, ed. A. M. Fowler, Vol. 3354, 566–578
- Monet, D. G., et al. 2003, *AJ*, 125, 984
- Morley, C. V., Fortney, J. J., Marley, M. S., Visscher, C., Saumon, D., & Leggett, S. 2012, *ApJ*, submitted
- Nakajima, T., Oppenheimer, B. R., Kulkarni, S. R., Golimowski, D. A., Matthews, K., & Durrance, S. T. 1995, *Nature*, 378, 463
- Oppenheimer, B. R., Kulkarni, S. R., Matthews, K., & Nakajima, T. 1995, *Science*, 270, 1478
- Pravdo, S. H., Shaklan, S. B., Wiktorowicz, S. J., Kulkarni, S., Lloyd, J. P., Martinache, F., Tuthill, P. G., & Ireland, M. J. 2006, *ApJ*, 649, 389
- Rayner, J. T., Toomey, D. W., Onaka, P. M., Denault, A. J., Stahlberger, W. E., Watanabe, D. Y., & Wang, S. 1998, in *Proc. SPIE: Infrared Astronomical Instrumentation*, ed. A. M. Fowler, Vol. 3354, 468–479
- Saumon, D., & Marley, M. S. 2008, *ApJ*, 689, 1327
- Saumon, D., Marley, M. S., Abel, M., Frommhold, L., & Freedman, R. S. 2012a, *ArXiv e-prints*
- . 2012b, *ApJ*, 750, 74
- Scholz, R.-D., Bihain, G., Schnurr, O., & Storm, J. 2011, *A&A*, 532, L5+
- Simons, D. A., & Tokunaga, A. 2002, *PASP*, 114, 169
- Spiegel, D. S., Burrows, A., & Milsom, J. A. 2010, *ArXiv e-prints*, (*ApJ*, in press)

- Stephens, D. C., & Leggett, S. K. 2004, PASP, 116, 9
- Tokunaga, A. T., Simons, D. A., & Vacca, W. D. 2002, PASP, 114, 180
- Vacca, W. D., Cushing, M. C., & Rayner, J. T. 2003, PASP, 115, 389
- van Dam, M. A., et al. 2006, PASP, 118, 310
- Warren, S., & Hewett, P. 2002, in Astronomical Society of the Pacific Conference Series, Vol. 283, A New Era in Cosmology, ed. N. Metcalfe & T. Shanks, 369
- Wizinowich, P. L., et al. 2006, PASP, 118, 297

WISE J1217+1626AB



WISE J1711+3500AB



CFBDSIR J1458+1013AB

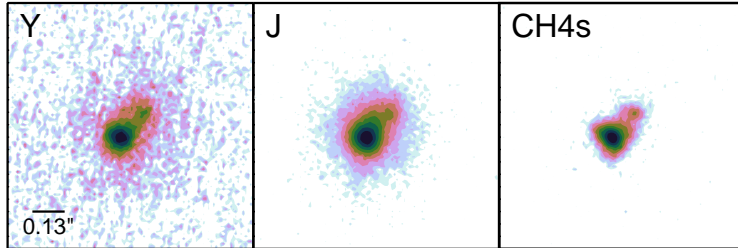


Fig. 1.— Keck LGS AO imaging of WISE J1217+1626AB, WISE J1711+3500AB, and CFBDSIR J1458+1013AB. North is up and east is left. The images of the *WISE* binaries are $2.0''$ on a side with colored contours plotted in uniform logarithmic intervals in flux, from 100% to 0.3% of the peak flux in each bandpass. The image of CFBDSIR J1458+1013AB is $1''$ on a side, with the lowest colored contour being 2% of the peak (since the fainter magnitude of this object results in a lower S/N dataset). For WISE J1217+1626AB, the $z_{1.1}$ -band image is not shown, but it is essentially identical to the *Y*-band one. The PSF halo of WISE J1217+1626AB is better detected than for the other two binaries because this dataset was obtained with NIRC2's most coarse pixel scale.

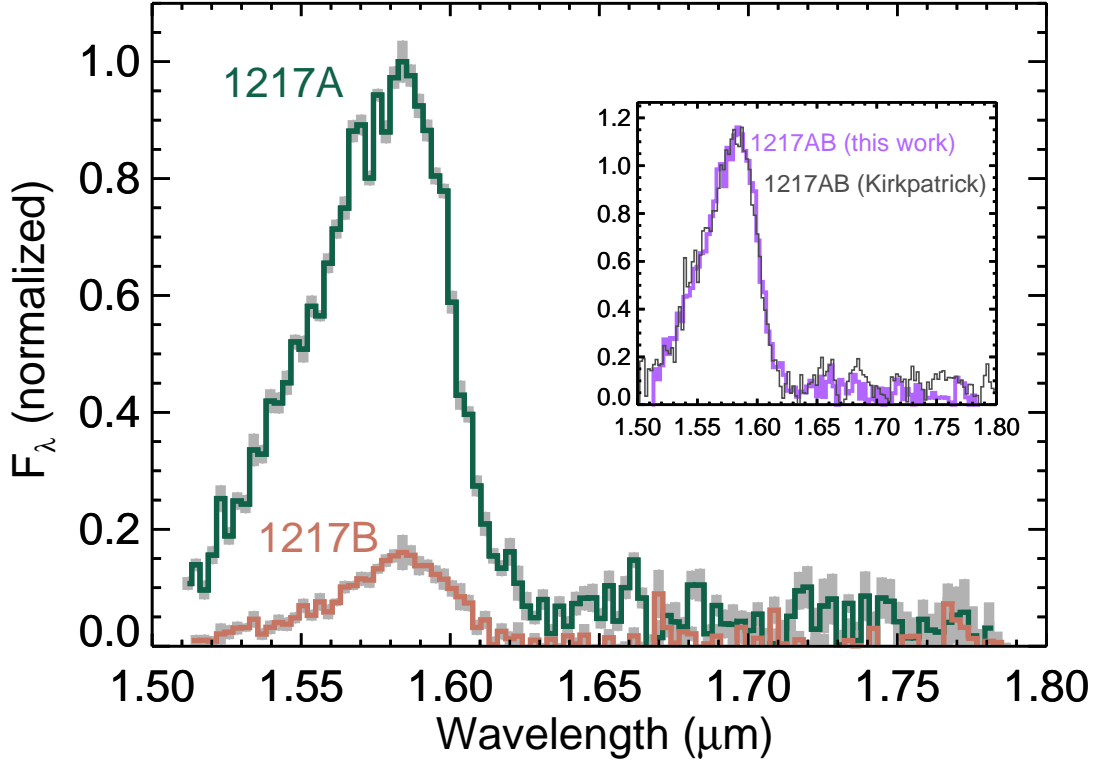


Fig. 2.— Keck/NIRSPEC H -band spectra of the two components of WISE J1217+1626AB, normalized to the peak flux of component A. The grey shaded histograms enswathing the spectra give the measurement uncertainties. The inset figure shows the sum of our NIRSPEC spectra for the components in purple, with the integrated-light spectrum from Kirkpatrick et al. (2011) shown in grey. The latter has been median smoothed by an 11-pixel box to boost its S/N and rebinned to comparable sampling as our NIRSPEC data.

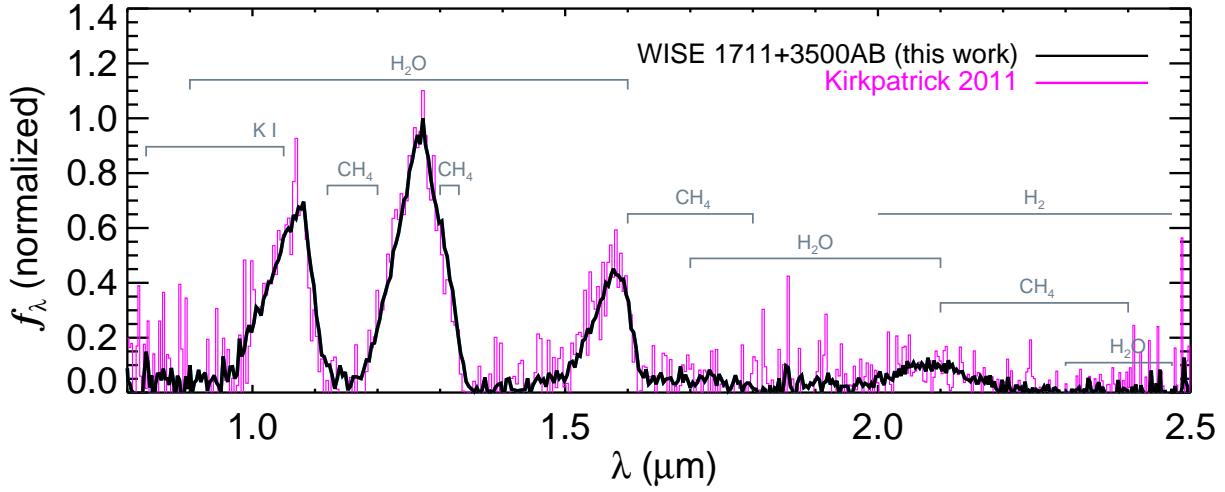


Fig. 3.— Our IRTF/SpeX integrated-light prism spectrum of WISE J1711+3500AB compared with that of Kirkpatrick et al. (2011). Major molecular features are marked in grey. The spectra are normalized to unity flux at the peak of their J -band continua.

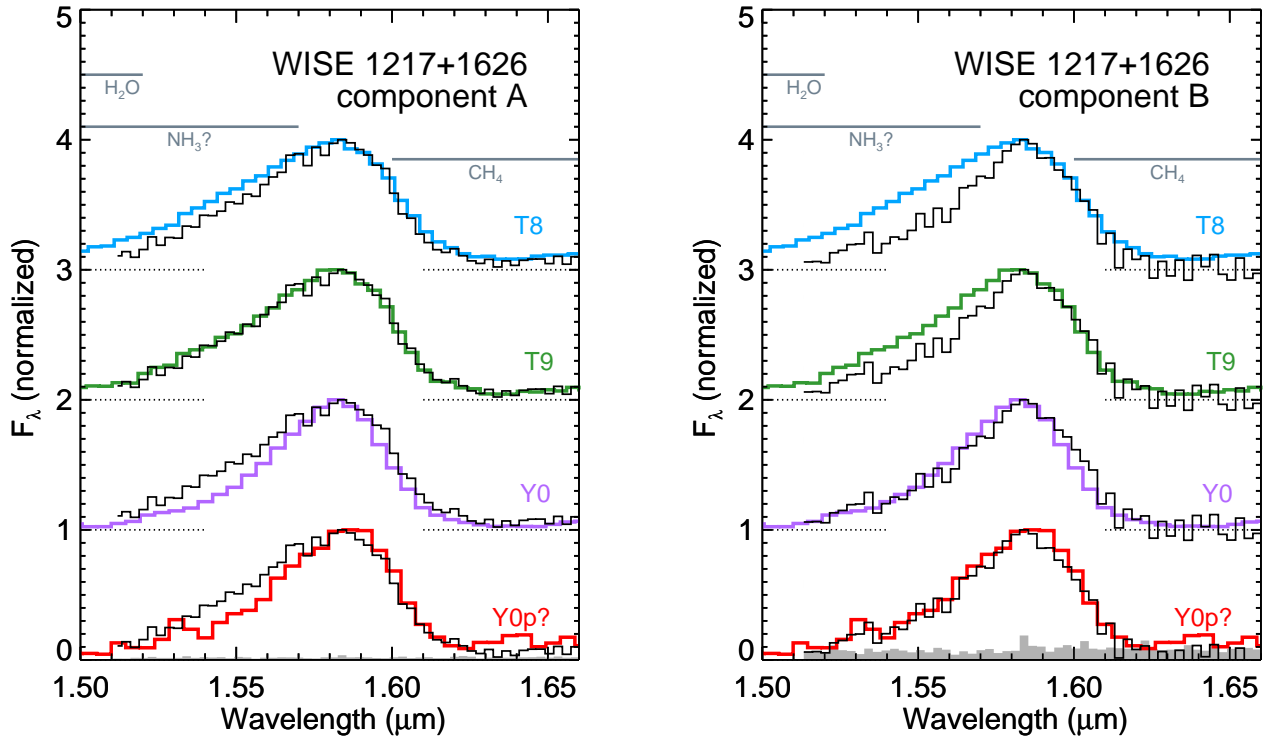


Fig. 4.— H -band spectra of the two components of WISE J1217+1626AB compared to spectral standards 2MASS J0415–0935 (T8), UGPS J0722–0540 (T9), and WISE J1738+2732 (Y0) as well as the peculiar Y0 WISE 1405+5534. All the spectra have been normalized to their peak flux. The grey shaded histogram at the bottom of each panel shows the measurement uncertainties for the WISE J1217+1626AB spectra.

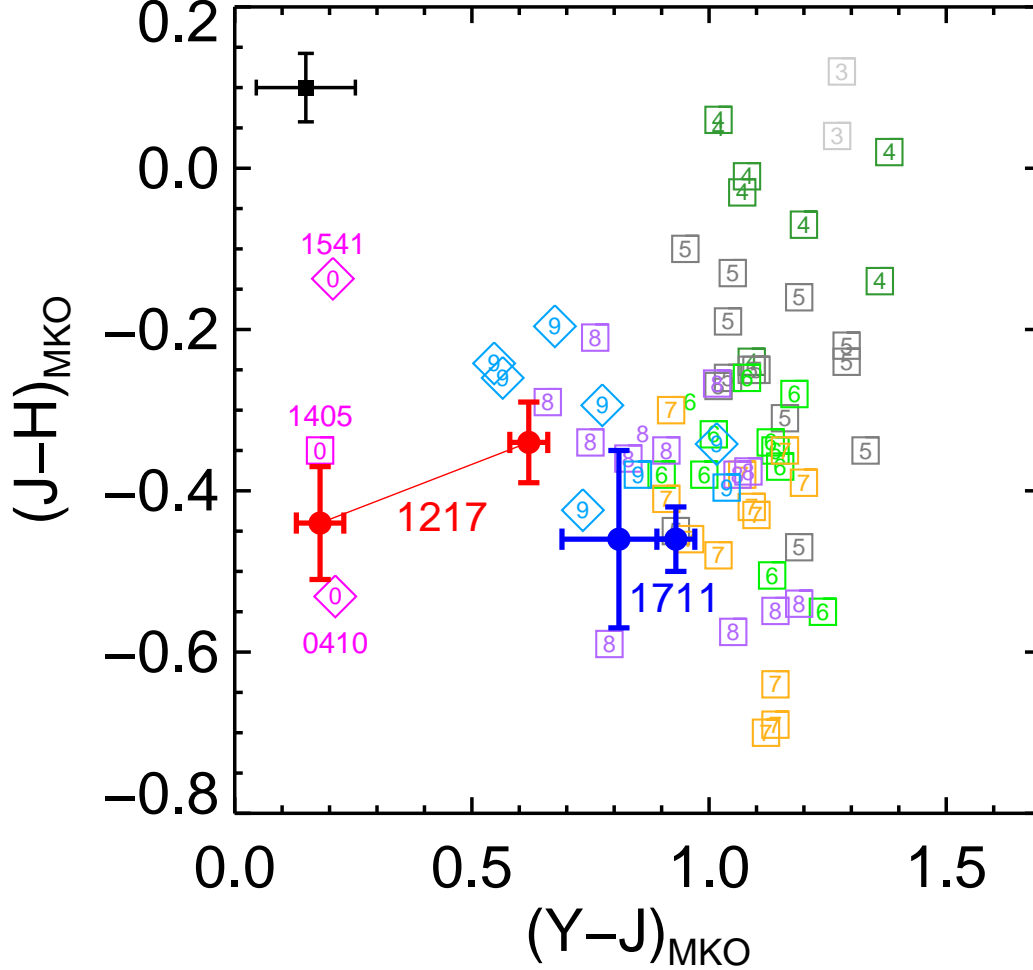


Fig. 5.— Resolved near-IR colors of WISE J1217+1626AB and WISE J1711+3500AB compared with published photometry of field T dwarfs (squares) and our synthetic photometry (diamonds) for T9–Y0 dwarfs. (See Section 3.4 for references.) For our *WISE* binaries, the secondary components for both systems are the points plotted to the left, being bluer in $Y - J$ than the primaries. (The resolved colors of CFBDSIR J1458+1013AB are consistent with the two *WISE* binaries, but are not plotted given their much larger uncertainties.) The plotted numbers indicate the near-IR subclass of the objects, with half subclasses being rounded down (e.g., “3” represents T3 and T3.5 dwarfs and “0” are the two Y0 dwarfs). Objects of the same subclass are also plotted in the same color. Known binaries are plotted as bare numbers without an encompassing square. The symbol in the upper left shows the median photometry errors for the field sample.

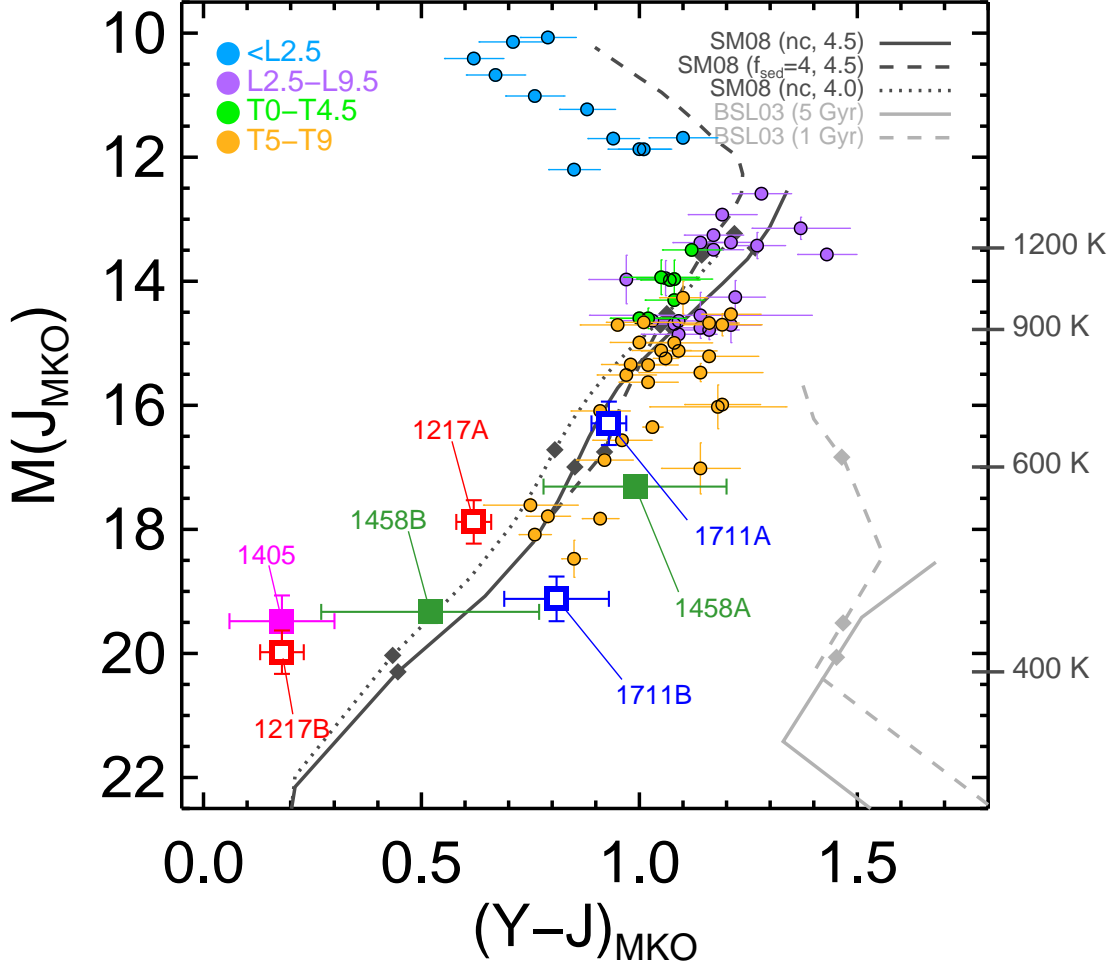


Fig. 6.— Near-IR color-magnitude diagram showing our binaries compared to field objects from the compilation of Dupuy & Liu (2012) and to evolutionary models of Burrows et al. (2003, light grey) and Saumon & Marley (2008, dark grey). For the *WISE* binaries (open squares), the positions are based on the photometric distances to the primary components, whereas CFBDSIR J1458+1013 and *WISE* J1405+5534 (filled squares) have parallactic distances from Dupuy & Liu (2012) and Kirkpatrick et al. (2012), respectively. The field sample only shows objects with parallax measurements of $S/N > 4$. For the Saumon & Marley models, we plot those that are cloud-free (“nc”; 350–1500 K) and that have a modest cloud layer ($f_{\text{sed}} = 4$; 500–2400 K) for $\log(g) = 4.0$ and 4.5 dex. The diamonds on the model tracks demarcate a common set of temperatures for all the models, and for the Saumon & Marley {nc, 4.5} models (dark grey solid line), the corresponding T_{eff} values are listed on the right hand axis.

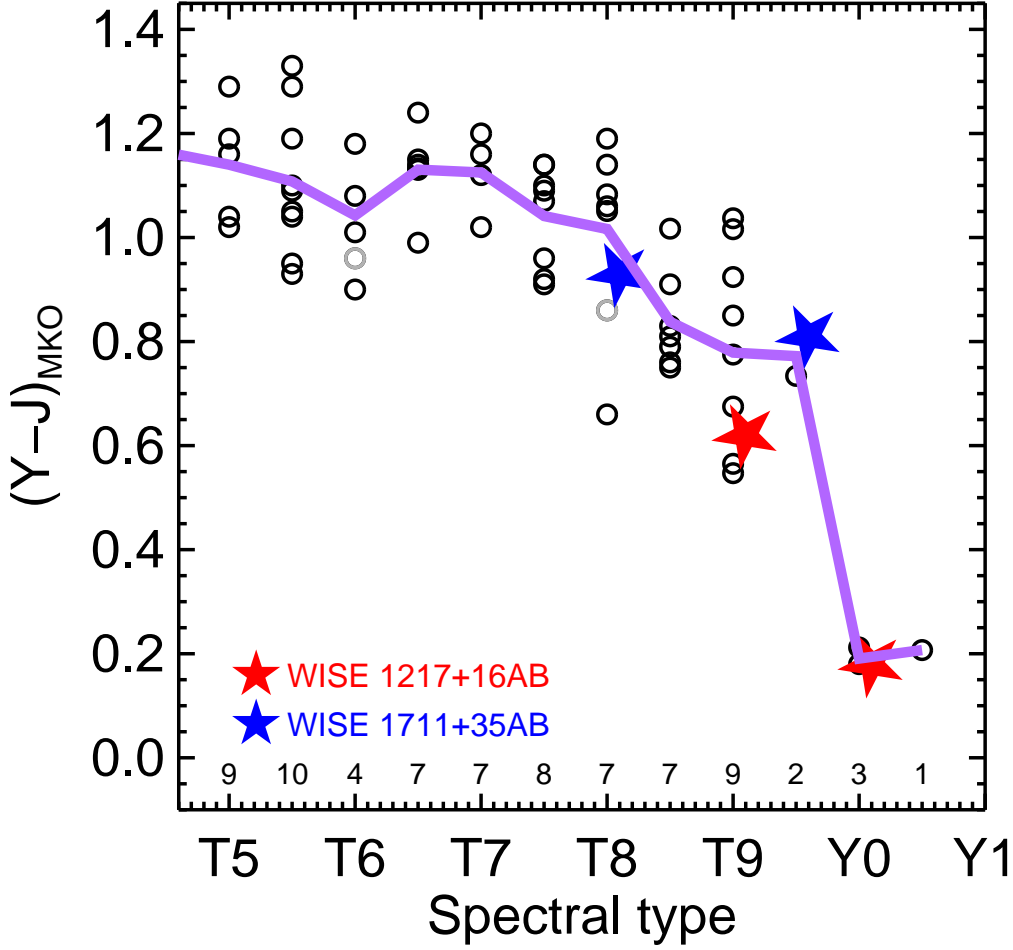


Fig. 7.— $(Y - J)$ color as a function of spectral type for the objects plotted in the previous color-color diagram (Figure 6). The median uncertainty for objects with published photometry is 0.10 mag. Known binaries are plotted in light grey. The components of our *WISE* binaries are slightly displaced horizontally from their actual spectra type for clarity. The purple line shows the average color as a function of spectral type, excluding known binaries. The small numbers at the bottom give the sample size used to compute the average color of each subclass. (The resolved colors of CFBDSIR J1458+1013AB are not plotted given their larger uncertainties but are consistent with objects of similar spectral type. However, as discussed in Section 3.4, the Y and J flux ratios for the system also show the large blue color difference between its primary and secondary component, like WISE J1217+1626AB does.)

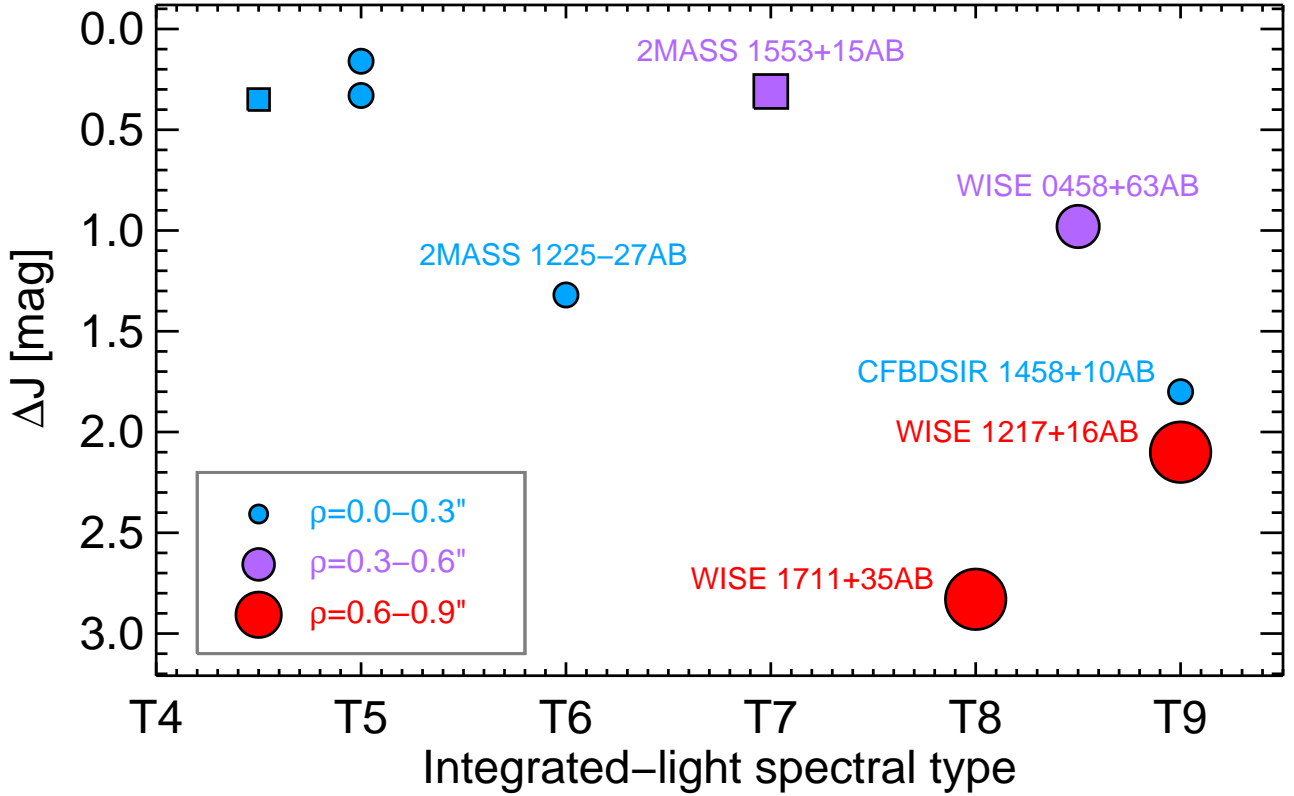


Fig. 8.— Integrated-light spectral type versus J -band flux ratio (a proxy for mass and temperature ratio) for known mid/late-T dwarf binaries, based on the compilation of Liu et al. (2010) and more recent discoveries by Liu et al. (2011) and Gelino et al. (2011). (For WISE J0458+63AB and CFBDSIR J1458+1013AB, we use the revised spectral types proposed by Cushing et al. 2011 of T8.5 and T9, respectively.) The plotting symbol sizes and colors represent the projected separation of the binaries. The circles represent ground-based photometry, either on the 2MASS or MKO system, and the squares represent objects with *HST*/NICMOS *F*110W photometry. Only CFBDSIR 1458+10AB (Liu et al. 2011) has comparably cold components to WISE J1217+1626AB and WISE J1711+3500AB, but it has a much tighter projected separation ($0.11''$).

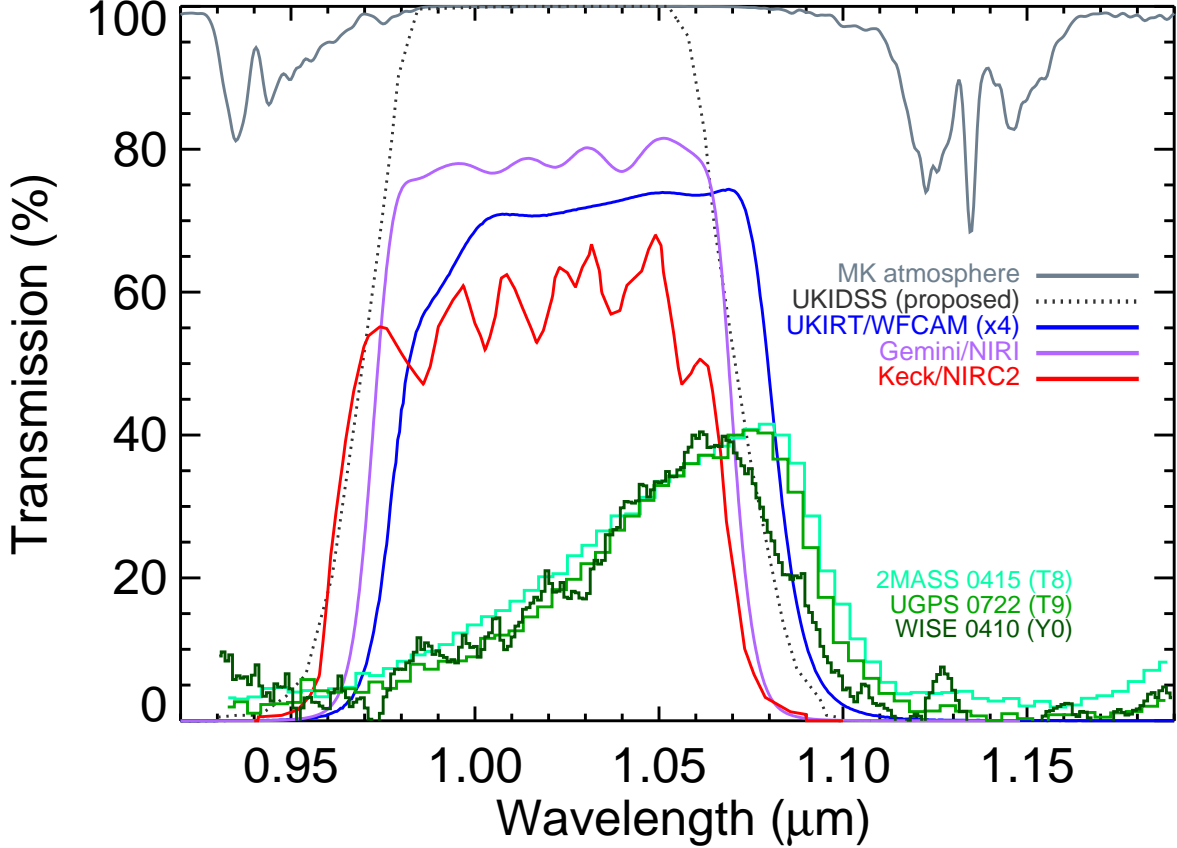


Fig. 9.— Comparison of the Y-band filters used in this work, from UKIRT/WFCAM, Gemini/NIRI, and Keck/NIRC2. The UKIRT/WFCAM curve represents the full combined transmission of the atmosphere, telescope, filter, and detector (Hewett et al. 2006) and has been multiplied by a factor of 4 to compare with the other two filters. The Gemini/NIRI and Keck/NIRC2 curves are the throughput of the filters only and were determined for 65 K and 77 K, respectively. We also show an atmospheric transmission model for the summit of Mauna Kea (from <http://www.jach.hawaii.edu/UKIRT/astronomy/utils/atmos-index.html>) and the original Y band proposed for UKIDSS (<http://www.ukidss.org>) based on Warren & Hewett (2002). The lower curves in green show the T8 and T9 spectroscopic standards and the Y0 dwarf WISE J0410+1502. (The Y0 standard WISE J1738+2732 of Cushing et al. 2011 does not have Y-band spectra). The spectrum of WISE J0410+1502 has been smoothed with a boxcar filter to boost the S/N, and all three spectra are not plotted below 0.93 μm , where their S/N is very low.

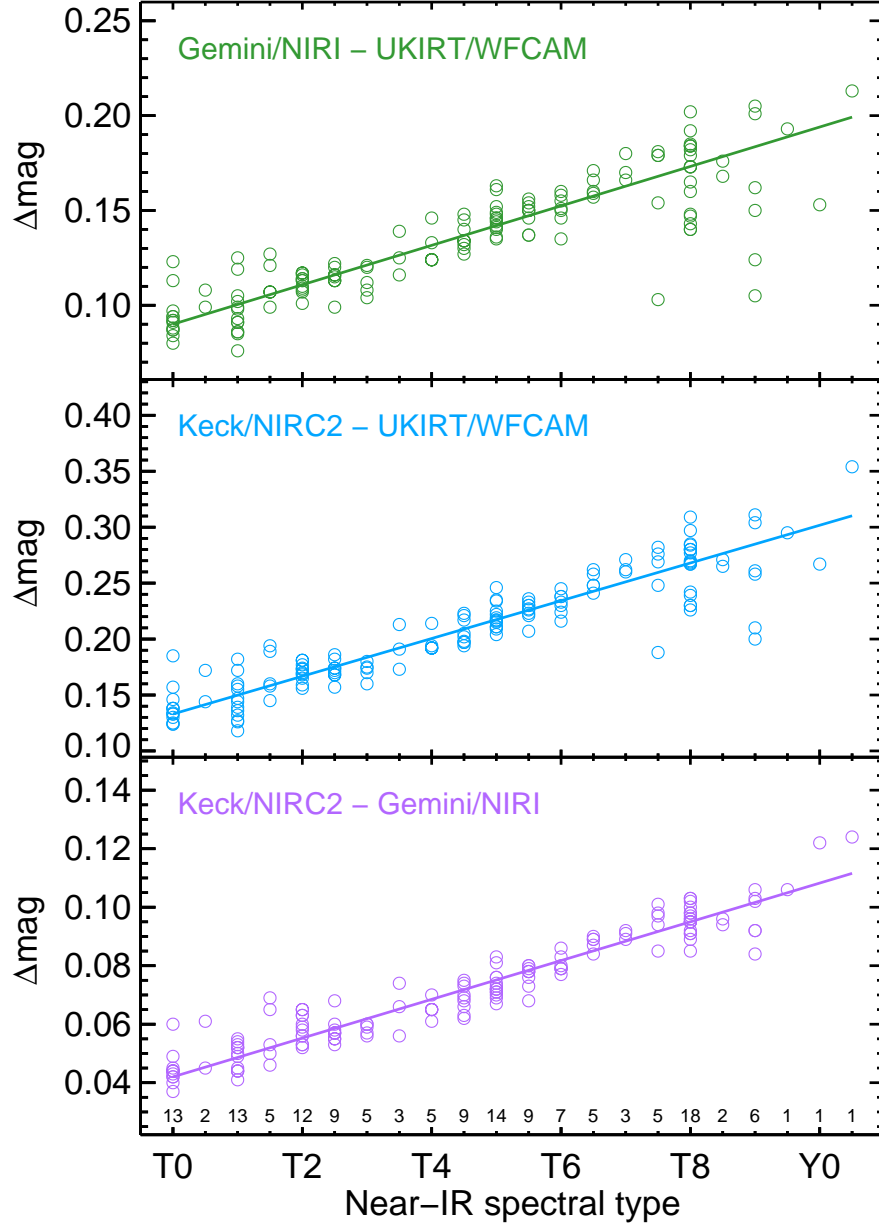


Fig. 10.— Synthesized offset between different Y-band filters for photometry of T and Y dwarfs. The label for each subplot gives the two relevant filters. Note that the S/N of the spectra for the T8–Y0.5 dwarfs is quite mixed, leading to scatter in the computed colors. The small row of numbers at the bottom gives the sample size for each subclass.

Table 1. Keck LGS AO Observations

Date (UT)	Filter ^a	$N_{images} \times T_{int}$ (s)	Airmass	FWHM (mas)	Strehl ratio	Separation (mas)	Position angle (deg)	Δmag
WISE J1217+1626AB								
2012-Jan-29	Y_{NIRC2}	6×180.0	1.03	130 ± 5	0.042 ± 0.003	758.2 ± 1.4 (1.2)	14.50 ± 0.13 (0.10)	1.666 ± 0.011
	$z_{1.1}$	6×300.0	1.12	144 ± 9	0.030 ± 0.006	759.2 ± 3.3 (3.2)	14.23 ± 0.26 (0.25)	1.69 ± 0.05
	J	7×60.0	1.01	115 ± 6	0.069 ± 0.007	757.1 ± 1.6 (1.5)	14.32 ± 0.10 (0.03)	2.10 ± 0.02
	$CH4s$	7×60.0	1.00	114 ± 6	0.087 ± 0.012	758.5 ± 1.9 (1.7)	14.43 ± 0.22 (0.20)	2.15 ± 0.04
	H	7×60.0	1.01	119 ± 10	0.082 ± 0.017	757.3 ± 2.5 (2.4)	14.37 ± 0.29 (0.27)	2.20 ± 0.04
	K	6×180.0	1.06	109 ± 3	0.17 ± 0.04	760.7 ± 6.2 (6.2)	14.27 ± 0.26 (0.24)	2.16 ± 0.13
WISE J1711+3500AB								
2012-Apr-12	Y_{NIRC2}	8×180.0	1.05	74 ± 7	0.025 ± 0.006	777.2 ± 8.1 (8.0)	328.74 ± 0.20 (0.19)	2.71 ± 0.11
	J	7×180.0	1.04	61 ± 6	0.059 ± 0.004	779.6 ± 1.1 (1.0)	328.40 ± 0.08 (0.07)	2.83 ± 0.06
	$CH4s$	8×120.0	1.04	55 ± 2	0.137 ± 0.018	779.8 ± 2.7 (2.6)	328.51 ± 0.19 (0.19)	2.63 ± 0.11
	H	8×120.0	1.04	56 ± 5	0.125 ± 0.006	780.0 ± 2.0 (1.9)	328.43 ± 0.23 (0.23)	2.83 ± 0.09
2012-Apr-13	K	5×180.0	1.04	60.0 ± 1.5	0.387 ± 0.107	780.7 ± 2.5 (2.4)	328.49 ± 0.09 (0.09)	3.08 ± 0.16
CFBDSIR J1458+1013AB								
2012-Apr-13	Y_{NIRC2}	5×180.0	1.07	65 ± 6	0.057 ± 0.040	125.6 ± 1.8 (1.8)	317.4 ± 1.3 (1.3)	1.55 ± 0.14
	J	3×180.0	1.03	73 ± 2	0.061 ± 0.008	127.2 ± 1.4 (1.4)	318.1 ± 1.1 (1.1)	2.02 ± 0.07
	$CH4s$	7×180.0	1.12	70 ± 6	0.178 ± 0.059	123.3 ± 2.2 (2.2)	317.8 ± 0.8 (0.8)	1.86 ± 0.13

Note. — JHK photometry is on the MKO system, while the Y -band filter is very similar to the UKIDSS filter but not the same. (See Appendix for details.) The uncertainties on the imaging performance (FWHM and Strehl ratio) are the RMS of the measurements from the individual images. For the separation and PA, the numbers in parenthesis are the RMS of the measurements before adding in the NIRC2 pixel scale and orientation uncertainties (i.e., the values relevant for computing the consistency of the astrometry between different filters).

Table 2. Properties of WISE J1217+1626AB

Property	Component A	Component B
Photometric distance (pc)		10.5 ± 1.7
Projected separation (AU)		8.0 ± 1.3
Y_{MKO} (mag)		18.38 ± 0.04
J_{MKO} (mag)		17.83 ± 0.02^a
H_{MKO} (mag)		18.18 ± 0.05^a
K_{MKO} (mag)		18.80 ± 0.04
Near-IR spectral type	T9 ± 0.5	Y0 ± 0.5
Y_{MKO} (mag)	18.59 ± 0.04	20.26 ± 0.04
J_{MKO} (mag)	17.98 ± 0.02	20.08 ± 0.03
H_{MKO} (mag)	18.31 ± 0.05	20.51 ± 0.06
K_{MKO} (mag)	18.94 ± 0.04	21.10 ± 0.12
$(Y - J)_{MKO}$ (mag)	0.62 ± 0.04	0.18 ± 0.05
$(J - H)_{MKO}$ (mag)	-0.34 ± 0.05	-0.44 ± 0.07
$(H - K)_{MKO}$ (mag)	-0.62 ± 0.07	-0.58 ± 0.14
$(J - K)_{MKO}$ (mag)	-0.96 ± 0.05	-1.02 ± 0.12
$M(Y_{MKO})$ (mag)	18.49 ± 0.35	20.16 ± 0.35
$M(J_{MKO})$ (mag)	17.88 ± 0.35	19.98 ± 0.35
$M(H_{MKO})$ (mag)	18.21 ± 0.35	20.41 ± 0.36
$M(K_{MKO})$ (mag)	18.84 ± 0.35	21.00 ± 0.37
$\log(L_{bol}/L_{\odot})$ [from J band]	-5.95 ± 0.18	-6.79 ± 0.18
$\log(L_{bol,B}/L_{bol,A})$ [from J band]		-0.84 ± 0.15
Evolutionary model results for 1.0 and 5.0 Gyr: Using Burrows et al. (2003) models and $M(J)$		
Mass (M_{Jup})	$11.5 \pm 1.1, 29 \pm 3$	$7.4 \pm 0.5, 18.4 \pm 1.0$
q ($\equiv M_B/M_A$)	$0.64 \pm 0.08, 0.63 \pm 0.08$	
$T_{eff}(K)$	$490 \pm 30, 530 \pm 30$	$381 \pm 13, 402 \pm 11$
$\log(g)$ (cgs)	$4.39 \pm 0.03, 4.95 \pm 0.05$	$4.18 \pm 0.03, 4.68 \pm 0.03$
Orbital period (yr)	$210^{+370}_{-50}, 130^{+230}_{-30}$	
Evolutionary model results for 1.0, 5.0 Gyr: Using Lyon/COND models and $M(J)$		
Mass (M_{Jup})	$14.4 \pm 1.8, 35 \pm 3$	$8.3 \pm 0.9, 20 \pm 2$
q ($\equiv M_B/M_A$)	$0.58 \pm 0.10, 0.57 \pm 0.08$	
$T_{eff}(K)$	$610 \pm 40, 660 \pm 40$	$430 \pm 30, 470 \pm 30$
$\log(g)$ (cgs)	$4.54 \pm 0.07, 5.07 \pm 0.05$	$4.27 \pm 0.05, 4.77 \pm 0.05$
Orbital period (yr)	$190^{+340}_{-50}, 120^{+220}_{-30}$	
Evolutionary model results for 1.0 and 5.0 Gyr: Using Lyon/COND models and L_{bol}		
Mass (M_{Jup})	$13 \pm 3, 33 \pm 5$	$5.5 \pm 1.2, 13 \pm 3$
q ($\equiv M_B/M_A$)	$0.42 \pm 0.22, 0.40 \pm 0.12$	
$T_{eff}(K)$	$580 \pm 70, 630 \pm 70$	$350 \pm 40, 370 \pm 50$
$\log(g)$ (cgs)	$4.47 \pm 0.10, 5.04 \pm 0.09$	$4.07 \pm 0.10, 4.54 \pm 0.11$
Orbital period (yr)	$210^{+380}_{-50}, 130^{+240}_{-30}$	

^aKirkpatrick et al. (2011)

Table 3. Properties of WISE J1711+3500AB

Property	Component A	Component B
Photometric distance (pc)		19 ± 3
Projected separation (AU)		15 ± 2
Y_{MKO} (mag)		18.51 ± 0.03^a
J_{MKO} (mag)		17.59 ± 0.03
H_{MKO} (mag)		18.05 ± 0.03^a
K_{MKO} (mag)		18.24 ± 0.03^a
Near-IR spectral type	$T8 \pm 0.5$	$(T9.5 \pm 0.5)^b$
Y_{MKO} (mag)	18.60 ± 0.03	21.31 ± 0.11
J_{MKO} (mag)	17.67 ± 0.03	20.50 ± 0.06
H_{MKO} (mag)	18.13 ± 0.03	20.96 ± 0.09
K_{MKO} (mag)	18.30 ± 0.03	21.38 ± 0.15
$(Y - J)_{MKO}$ (mag)	0.93 ± 0.04	0.81 ± 0.12
$(J - H)_{MKO}$ (mag)	-0.46 ± 0.04	-0.46 ± 0.11
$(H - K)_{MKO}$ (mag)	-0.17 ± 0.04	-0.42 ± 0.18
$(J - K)_{MKO}$ (mag)	-0.63 ± 0.04	-0.88 ± 0.17
$M(Y_{MKO})$ (mag)	17.22 ± 0.35	19.93 ± 0.37
$M(J_{MKO})$ (mag)	16.29 ± 0.35	19.12 ± 0.36
$M(H_{MKO})$ (mag)	16.75 ± 0.35	19.58 ± 0.36
$M(K_{MKO})$ (mag)	16.92 ± 0.35	20.00 ± 0.38
$\log(L_{bol}/L_{\odot})$ [from J band]	-5.60 ± 0.17	-6.45 ± 0.18
$\log(L_{bol,B}/L_{bol,A})$ [from J band]		-0.84 ± 0.15
Evolutionary model results for 1.0 and 5.0 Gyr: Using Burrows et al. (2003) models and $M(J)$		
Mass (M_{Jup})	$19 \pm 3, 44 \pm 4$	$8.7 \pm 0.8, 22 \pm 2$
q ($\equiv M_B/M_A$)	$0.46 \pm 0.09, 0.50 \pm 0.07$	
$T_{eff}(K)$	$675 \pm 50, 680 \pm 40$	$420 \pm 20, 440 \pm 30$
$\log(g)$ (cgs)	$4.65 \pm 0.07, 5.18 \pm 0.05$	$4.26 \pm 0.03, 4.76 \pm 0.05$
Orbital period (yr)	$430^{+770}_{-100}, 280^{+500}_{-70}$	
Evolutionary model results for 1.0, 5.0 Gyr: Using Lyon/COND models and $M(J)$		
Mass (M_{Jup})	$23 \pm 2, 48 \pm 3$	$10.7 \pm 0.9, 26 \pm 2$
q ($\equiv M_B/M_A$)	$0.46 \pm 0.06, 0.54 \pm 0.05$	
$T_{eff}(K)$	$810 \pm 50, 870 \pm 60$	$500 \pm 30, 540 \pm 30$
$\log(g)$ (cgs)	$4.78 \pm 0.05, 5.27 \pm 0.04$	$4.39 \pm 0.04, 4.90 \pm 0.05$
Orbital period (yr)	$390^{+700}_{-90}, 260^{+480}_{-60}$	
Evolutionary model results for 1.0 and 5.0 Gyr: Using Lyon/COND models and L_{bol}		
Mass (M_{Jup})	$19 \pm 3, 44 \pm 6$	$8.1 \pm 1.6, 20 \pm 4$
q ($\equiv M_B/M_A$)	$0.43 \pm 0.12, 0.45 \pm 0.12$	
$T_{eff}(K)$	$730 \pm 80, 800 \pm 90$	$430 \pm 50, 460 \pm 50$
$\log(g)$ (cgs)	$4.70 \pm 0.09, 5.21 \pm 0.08$	$4.26 \pm 0.10, 4.76 \pm 0.10$
Orbital period (yr)	$430^{+780}_{-110}, 280^{+510}_{-70}$	

^aSynthesized from our J -band photometry and IRTF/SpeX spectrum (Section 2.4).

^bEstimated from H -band absolute magnitude (Section 3.3).

Table 4. Resolved Photometry of CFBDSIR J1458+1013AB

Property	Component A	Component B
Distance (pc)	$31.9 \pm 2.5^{\text{a}}$	
Projected separation (AU)	$3.5 \pm 0.3^{\text{b}}$	
Y_{MKO} (mag)	$20.58 \pm 0.21^{\text{c}}$	
J_{MKO} (mag)	$19.67 \pm 0.02^{\text{d}}$	
H_{MKO} (mag)	$20.06 \pm 0.10^{\text{d}}$	
K_{MKO} (mag)	$20.50 \pm 0.24^{\text{d}}$	
Near-IR spectral type	$\text{T9} \pm 0.5^{\text{e}}$	$(\text{Y0} \pm 0.5)^{\text{f}}$
Y_{MKO} (mag)	20.81 ± 0.21	22.36 ± 0.24
J_{MKO} (mag)	19.83 ± 0.02	21.85 ± 0.06
H_{MKO} (mag)	20.18 ± 0.10	22.51 ± 0.16
K_{MKO} (mag)	20.63 ± 0.24	22.83 ± 0.30
$(Y - J)_{MKO}$ (mag)	0.99 ± 0.21	0.52 ± 0.25
$(J - H)_{MKO}$ (mag)	-0.35 ± 0.10	-0.66 ± 0.17
$(H - K)_{MKO}$ (mag)	-0.45 ± 0.26	-0.32 ± 0.34
$(J - K)_{MKO}$ (mag)	-0.81 ± 0.24	-0.99 ± 0.30
$M(Y_{MKO})$ (mag)	18.29 ± 0.27	19.84 ± 0.29
$M(J_{MKO})$ (mag)	17.31 ± 0.17	19.33 ± 0.18
$M(H_{MKO})$ (mag)	17.66 ± 0.20	19.99 ± 0.23
$M(K_{MKO})$ (mag)	18.11 ± 0.30	20.31 ± 0.34
$\log(L_{\text{bol}}/L_{\odot})$ [from J band]	-5.72 ± 0.13	-6.53 ± 0.13
$\log(L_{\text{bol},B}/L_{\text{bol},A})$ [from J band]	-0.81 ± 0.15	

^aDupuy & Liu (2012)

^bEpoch 2010 July 08 UT

^cUKIDSS Data Release 8

^dDelorme et al. (2010)

^eClassification by Cushing et al. (2011) based on Liu et al. (2011) spectrum.

^fEstimated from H -band absolute magnitude (Section 3.3).

Note. — Resolved Y - and J -band photometry based on new flux ratio measurements in this paper, while the flux ratios in the other bandpasses and all the integrated-light photometry come from Liu et al. (2011).

Table 5. UKIDSS DR9 Photometry of *WISE* Brown Dwarfs

Object	Ref.	SpT	Y_{MKO} (mag)	J_{MKO} (mag)	H_{MKO} (mag)	K_{MKO} (mag)
WISE J0049+0441	1	L9	16.903 ± 0.012	15.767 ± 0.007	14.801 ± 0.006	14.131 ± 0.005
WISE J0254+0223 ^a	2,3	T8	16.999 ± 0.014	15.916 ± 0.008	16.29 ± 0.02	16.73 ± 0.05
WISE J0750+2725	1	T8.5	19.75 ± 0.09	18.73 ± 0.05	19.00 ± 0.06^b	...
WISE J0929+0409	1	T6.5	18.00 ± 0.02	16.87 ± 0.014	17.37 ± 0.07	17.40 ± 0.09
WISE J1311+0122	1	T9	19.89 ± 0.10	18.97 ± 0.08
WISE J2226+0440	1	T8	18.04 ± 0.03	16.899 ± 0.019	17.45 ± 0.07	17.24 ± 0.09
WISE J2344+1034	1	T9	19.88 ± 0.12	18.84 ± 0.09	19.24 ± 0.29	...

^aa.k.a. PSO J043.5+02

^b*H*-band photometry from Kirkpatrick et al. (2011).

References. — (1) Kirkpatrick et al. (2011), (2) Liu et al. (2011), (3) Scholz et al. (2011).